Helsinki University of Technology
Department of Electrical and Communications Engineering
Optoelectronics Laboratory

Growth and properties of GaAsN structures

Juha Toivonen

Dissertation for the degree of Doctor of Science in Technology to be presented with due permission of the Department of Electrical and Communications Engineering, for public examination and debate in Auditorium S4 at Helsinki University of Technology (Espoo, Finland) on the 16th of May, 2003, at 12 o'clock noon.

Espoo, Finland
2003

Distribution:
Helsinki University of Technology
Department of Electrical and Communications Engineering
Optoelectronics Laboratory
P.O.Box 3500
FIN-02015 HUT
FINLAND
Tel: +358 9 451 3121
Fax: +358 9 451 3128
This dissertation can be read at http://lib.hut.fi/Diss/

ISBN 951-22-6436-6 (printed version)
ISBN 951-22-6437-4 (electronic version)

Picaset Oy
Helsinki 2003

ABSTRACT

Recently, the addition of nitrogen into GaAs-based components has attracted considerable attention due to the high potential of the technique in many device applications. The N incorporation from dimethylhydrazine into $GaAs_{1-x}N_x$ by metalorganic vapor phase epitaxy (MOVPE) was studied in this thesis. The incorporation efficiency of N into GaAs is very low and thus carefully optimized growth conditions are required. The electrical, structural, and optical properties of $GaAs_{1-x}N_x$ were investigated with various experimental techniques. The luminescence intensity of the material degrades rapidly with increasing N composition due to the formation of nonradiative point defects. However, post-growth treatments, like laser treatment or annealing, can be used to recover the luminescence intensity.

A record high N composition x of 0.056 for MOVPE-grown $GaAs_{1-x}N_x$ was achieved by optimizing the growth conditions. Post-growth treatments were studied for optimum luminescence intensity. Comparable results were gained using annealing at 700°C for 10 minutes and laser treatment with the laser intensity of 10 kW/cm^2 for one minute. Similar growth and post-growth treatment conditions were applied to $Ga_{1-y}In_yN_xAs_{1-x}$ quantum well structures. Annealing was found to shift the transition energy of $Ga_{1-y}In_yN_xAs_{1-x}$ by up to 100 meV toward higher energies due to the local rearrangement of N neighboring atoms, whereas a negligible shift was observed after the laser treatment.

The critical thickness for misfit dislocation formation of $GaAs_{1-x}N_x$ on GaAs was studied with synchrotron x-ray topography. The critical thickness was found to be about twice as large as the theoretical prediction. Point defects in $GaAs_{1-x}N_x$ were investigated using positron annihilation spectroscopy. An increasing concentration of Ga vacancies was found when the N composition x was increased. The anticorrelation between the luminescence intensity and the vacancy concentration was attributed to nonradiative recombination through the defect complexes containing the Ga vacancies.

PREFACE

The work presented in this thesis has been carried out at the Optoelectronics Laboratory of Helsinki University of Technology during 1999–2002.

I want to express my gratitude to Professor Turkka Tuomi, the supervisor of this thesis, for an opportunity to work in the interesting field of semiconductor epitaxy and characterization, and for his support during these years. I am indebted to Professor Harri Lipsanen, who initiated the research on arsenide-nitrides at the Optoelectronics Laboratory and has instructed me in several experimental techniques during this work. I want to thank Dr. Markku Sopanen for his advice in epitaxy and for his help with the manuscripts. I am grateful to Teppo Hakkarainen for the fruitful collaboration in studies on arsenide-nitrides.

I want to thank the personnel of the laboratory, especially Dr. Reko Rantamäki, Karri Varis, Lauri Knuuttila, Juha Riikonen, Marco Mattila, Jaakko Sormunen, Pasi Kostamo, and Outi Reentilä for the cooperation. I am grateful for the collaboration with the Physics Laboratory, particularly I want to thank Dr. Juha Oila for performing the positron annihilation measurements and Professor Kimmo Saarinen for the help with the manuscript. I am grateful to the people of the collaborating research groups at other universities, D. Lowney, J. Kanatharana, W. Chen, and Prof. P. J. McNally at Microelectronics Research Laboratory in Dublin, Ireland, and Dr. W. Li and Prof. M. Pessa at Optoelectronics Research Center, Finland.

The Graduate School of Electronics Manufacturing and the Finnish Cultural Foundation are acknowledged for the financial support of this work.

I want to thank my fiancée Leena for her support and patience during this work, and my parents for their continuous encouragement.

Espoo, January 2003 Juha Toivonen

LIST OF PUBLICATIONS

This thesis consist of an overview and the following publications:

I J. Toivonen, T. Hakkarainen, M. Sopanen, and H. Lipsanen, *High nitrogen composition GaAsN by atmospheric pressure metalorganic vapor-phase epitaxy*, Journal of Crystal Growth **221**, 456–460 (2000).

II W. Li, M. Pessa, J. Toivonen, and H. Lipsanen, *Doping and carrier transport in $Ga_{1-3x}In_{3x}N_xAs_{1-x}$ alloys*, Physical Review B **64**, 113308 1–4 (2001).

III T. Hakkarainen, J. Toivonen, M. Sopanen, and H. Lipsanen, *Self-assembled GaIn(N)As quantum dots: Enhanced luminescence at 1.3 μm*, Applied Physics Letters **79**, 3932–3934 (2001).

IV T. Hakkarainen, J. Toivonen, M. Sopanen, and H. Lipsanen, *GaInNAs quantum well structures for 1.55 μm emission on GaAs by atmospheric pressure metalorganic vapor phase epitaxy*, Journal of Crystal Growth **234**, 631–636 (2002).

V T. Hakkarainen, J. Toivonen, M. Sopanen, and H. Lipsanen, *Wavelength extension of GaInAs/GaIn(N)As quantum dot structures grown on GaAs*, Journal of Crystal Growth **248**, 339–342 (2003).

VI J. Toivonen, T. Tuomi, J. Riikonen, L. Knuuttila, T. Hakkarainen, M. Sopanen, H. Lipsanen, P. J. McNally, W. Chen, and D. Lowney, *Misfit dislocations in GaAsN - GaAs interface*, accepted to Journal of Materials Science: Materials in Electronics.

VII J. Toivonen, T. Hakkarainen, M. Sopanen, H. Lipsanen, J. Oila, and K. Saarinen, *Observation of defect complexes containing Ga vacancies in GaAsN*, Applied Physics Letters **82**, 40–42 (2003).

VIII J. Toivonen, T. Hakkarainen, M. Sopanen, and H. Lipsanen, *Effect of post-growth laser treatment on optical properties of Ga(In)NAs quantum wells*, IEE Proceedings – Optoelectronics **150**, 68–71 (2003).

AUTHOR'S CONTRIBUTION

The author has contributed to the data analysis for publications I–VIII. He has written the manuscripts for publications I, VI–VIII and has contributed to the manuscripts for publications III–V.

The sample structures and growth parameters for publications I, III–VIII were planned by the author, T. Hakkarainen, and Dr. M. Sopanen. The samples for publications I, VI, VII and VIII were grown mainly by the author.

The author has performed the optical measurements for publications I, II, VI–VIII. The x-ray diffraction studies for publications I, VI–VIII were performed by the author. The synchrotron x-ray topography study for publication VI was performed by the author and assisted by the co-authors of publication.

The optical microscopy and atomic force microscopy for publication VI and the Hall measurements for publication VII were performed by the author.

CONTENTS

PREFACE ..... **v**
LIST OF PUBLICATIONS ..... **vi**
AUTHOR'S CONTRIBUTION ..... **vii**
1 INTRODUCTION **1**
2 FUNDAMENTALS OF GaAsN **4**
2.1 Anomalous properties 4
2.2 Impurity and alloy limits 6
2.3 Band anticrossing model 8
2.4 Pseudopotential method 12
3 EPITAXIAL GROWTH **14**
3.1 Metalorganic vapor phase epitaxy 14
3.2 Precursors 16
3.3 Temperature 18
3.4 Growth rate 20
3.5 V/III-ratio 20
3.6 Pressure and carrier gas 21
3.7 MOVPE vs. MBE 22
4 STRUCTURAL PROPERTIES **24**
4.1 Surface morphology 24
4.2 Misfit dislocations 25
4.3 Point defects 28
4.4 Gallium vacancies 29
5 OPTICAL PROPERTIES **32**
5.1 Luminescence 32
5.2 Post-growth treatments 34
5.3 Photoreflectance 37
6 GaInNAs **38**
6.1 Bulk layers 38
6.2 Quantum wells 40
6.3 Quantum dots 41
7 SUMMARY **43**
REFERENCES **45**

1 INTRODUCTION

Optical communications use quartz fibers as the transportation media of light. The most widely used single-mode optical fiber has a chromatic dispersion minimum at a wavelength of 1300 nm and an attenuation minimum at 1550 nm. It also has local attenuation minima at 850 nm and 1300 nm. The properties of the optical fiber have fixed these wavelengths as the optical communications wavelengths.

Semiconductor lasers are used as emitters in optical communications. Indium phosphide (InP) based lasers are used for the wavelengths of 1300 nm and 1550 nm. For the wavelength of 850 nm, more inexpensive gallium arsenide (GaAs) based lasers are used. GaAs also enables the use of a vertical cavity surface-emitting laser (VCSEL), a cost effective laser structure, where the laser light comes out from the top or the bottom surface of the laser. Since the mid 1990's, these gigahertz VCSELs operating at 850 nm have rapidly replaced conventional edge-emitting lasers in short-range optical telecommunication. With an optical link distance of over 300 m and 20 km, the wavelengths of 1300 nm and 1550 nm are used in lasers, respectively. Thus, for several years there has been a lot of activity in developing GaAs-based active material for these wavelengths to realize a long-wavelength VCSEL.

A promising candidate for a long-wavelength operation on GaAs is the use of In(Ga)As quantum dot structures [1]. However, the commercial breakthrough has not occurred yet. Another approach was introduced in 1992, when Weyers, Sato, and Ando [2] reported a significant red shift of the wavelength when a small fraction of nitrogen was alloyed into GaAs to form a ternary alloy $GaAs_{1-x}N_x$. Later, in 1996, Kondow et al. [3] proposed a novel quaternary material $Ga_{1-y}In_yN_xAs_{1-x}$, which would enable long-wavelength lasers on GaAs. The development of a GaAs based VCSEL utilizing $Ga_{1-y}In_yN_xAs_{1-x}$ as the active material and operating at 1300 nm has been rapid [4], and the first commercial products are about to arise. These components will enable a cost-effective high-speed data transfer for intermediate distances of up to 20 km.

Figure 1 shows the band gaps of semiconductors that are typically used in telecommunication lasers. Suitable substrate materials are GaAs and InP. The component structures have to be grown coherently on the substrate, and thus the lattice constants of the grown materials need to be about the same as in the substrate. The shaded areas in figure 1 approximate the tuning ranges for the band gap of $Ga_{1-y}In_yN_xAs_{1-x}$ and $Ga_{1-y}In_yP_xAs_{1-x}$ layers on GaAs and InP,

respectively. The two alloys cover about the same wavelength ranges. The $Ga_{1-y}In_yN_xAs_{1-x}$ on GaAs material combination has many advantages over widely used $Ga_{1-y}In_yP_xAs_{1-x}$ on InP for the communications lasers, like better temperature stability due to stronger carrier confinement, lower manufacturing costs, and compatibility with the mature VCSEL structure. However, the relatively new $Ga_{1-y}In_yN_xAs_{1-x}$ compound still suffers from the degradation of electrical and optical properties as the N composition x is increased. Challenges remain in the understanding of the growth and the physics of the compound.

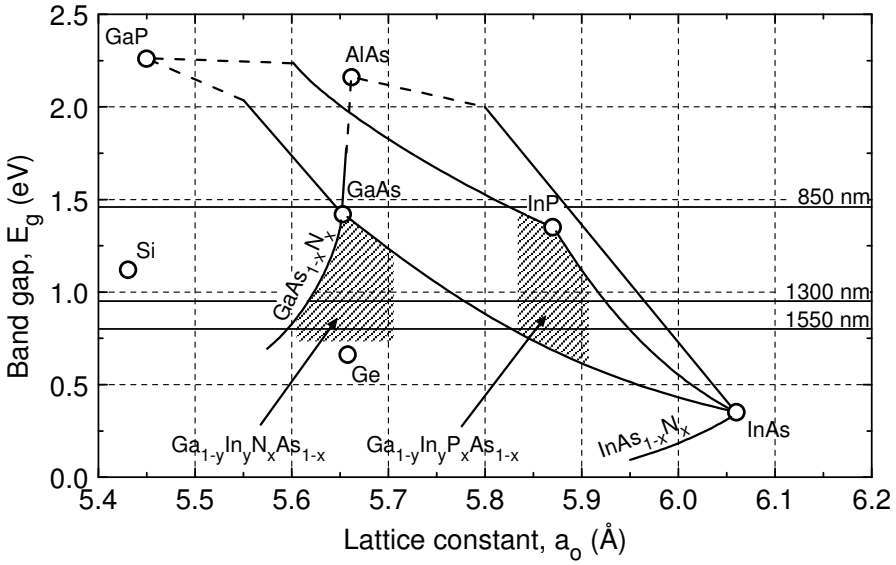

Figure 1. Band gaps of selected semiconductors as a function of lattice constant. Continuous and dashed lines indicate direct and indirect band gaps, respectively. Shaded areas show tunable wavelength ranges of $Ga_{1-y}In_yN_xAs_{1-x}$ on GaAs and $Ga_{1-y}In_yP_xAs_{1-x}$ on InP substrates.

In this thesis, the properties of Ga(In)NAs layers and nanostructures have been studied. The Ga(In)NAs samples were grown using metalorganic vapor phase epitaxy, except for publication II, wherein the electrical properties of lattice matched GaInNAs on GaAs were studied with samples grown by molecular beam epitaxy. In publications I and IV the growth and annealing conditions of $GaAs_{1-x}N_x$ and $Ga_{1-y}In_yN_xAs_{1-x}$ quantum well structures for long-wavelength emission on GaAs were optimized. An emission at the communications wavelengths was achieved. The combination of quantum dot structures and $Ga_{1-y}In_yN_xAs_{1-x}$ for long-wavelength emission was studied in publications III and V. An enhanced luminescence intensity was observed at the wavelength of 1300 nm.

The structural properties of $GaAs_{1-x}N_x$ layers on GaAs were studied with atomic force microscopy, x-ray diffraction, and synchrotron x-ray topography. A

good structural quality of $GaAs_{1-x}N_x$ layers was observed when the layer thickness was smaller than the critical thickness. The critical thickness is understood as a maximum layer thickness, which can be grown on substrate material without strain induced lattice defects. In publication VI the critical thickness is determined and the strain in the layers thicker than the critical thickness was found to relax through dislocations and cracks. Vacancy defects in $GaAs_{1-x}N_x$ were studied in publication VII with positron annihilation spectroscopy. An increasing concentration of Ga vacancies was found with increasing N composition x. The anticorrelation between the photoluminescence intensity and the vacancy concentration was attributed to nonradiative recombination through the defect complexes containing Ga vacancies. In publication VIII the effect of post-growth laser treatment on Ga(In)NAs quantum wells was studied. Laser treatment was found to be as effective as annealing to recover the photoluminescence intensity of $GaAs_{1-x}N_x$. A negligible blue shift was observed for $Ga_{1-y}In_yN_xAs_{1-x}$ after the laser treatment as compared to that after annealing. The negligible blue shift is advantageous when reaching long wavelengths.

The structure of this overview is the following. The experimental findings and theoretical studies on $GaAs_{1-x}N_x$ are reviewed in chapter 2. In the following chapters the results of publications I–VIII are discussed together with the reviews of the specific issues. Chapter 3 introduces epitaxial growth techniques and discusses the growth conditions needed for epitaxy of $GaAs_{1-x}N_x$. Chapter 4 discusses the structural properties of $GaAs_{1-x}N_x$ and introduces the experimental methods used in the studies. The optical properties of the material and the effect of post-growth treatments on those are discussed in chapter 5. Quaternary alloy $Ga_{1-y}In_yN_xAs_{1-x}$ is introduced in chapter 6 and the use of the alloy in quantum dot structures is discussed. A short review of the device applications of the alloy is given. Finally, chapter 7 summarizes the main results of this thesis.

2 FUNDAMENTALS OF GaAsN

It has been possible to grow $GaAs_{1-x}N_x$ with the composition x of a few per cent on GaAs substrates for several years. However, the basic parameters, like conduction band and valence band energies, band offsets, effective masses and lattice constant of the compound are not well known and the results of different research groups are inconsistent. This is due to the difficult growth conditions and the very exceptional physical properties of the alloy. Section 2.1 introduces these anomalous properties, and section 2.2 discusses more carefully the experimentally observed properties of the compound in dilute and in alloy limits. Sections 2.3 and 2.4 describe two theoretical models: the band anticrossing model and the pseudopotential theory.

2.1 Anomalous properties

In a typical isovalent AB_xC_{1-x} compound semiconductor, the properties of AB_xC_{1-x} change gradually from the properties of the material AC to the properties of the material AB as the composition x is increased from 0 to 1. Most of the material parameters change linearly with composition. Two important parameters of common semiconductors, band gap energy E_g and lattice constant a_o, are shown in figure 1 in chapter 1. The lattice constant behaves linearly with composition x. The linear behavior of lattice constant is known as the Vegard's law. The band gap energy usually exhibits nonlinear bowing, and the change in the band gap energy is expressed as

$$E_{g,ABC}(x) = x \cdot E_{g,AB} + (1-x) \cdot E_{g,AC} - b \cdot x \cdot (1-x), \qquad (1)$$

where b is a bowing coefficient. The value of b is usually less than 1 eV and it is composition-independent. The band gap energy changes with composition also in dilute regime ($x < 0.01$) as equation 1 describes.

It was early noticed that $GaAs_{1-x}N_x$, does not behave as a typical isovalent alloy. An isolated N atom in a GaAs lattice was observed to form a localized electron state above the conduction band and to act as an excitonic recombination channel under hydrostatic pressure [5]. Later, in 1990, Liu et al. reported about N clusters below the conduction band of GaAs [6, 7]. Thus, $GaAs_{1-x}N_x$ is not behaving as a normal isovalent alloy in dilute compositions, but N forms localized and optically active electron states near the conduction band of GaAs. In 1992, Weyers et al. were able to grow $GaAs_{1-x}N_x$ alloy with the N composition x of up to 0.016 [2, 8]. They observed a significant red shift of

band-edge emission and absorption. Relying on a linear approximation, one would expect an increase of the band gap energy from 1.42 eV of GaAs toward 3.2 eV of cubic GaN with increasing N composition x. The decrease of the band gap with increasing N composition x means a huge bowing of the band gap energy.

Figure 2 shows the band alignment of GaAs and cubic GaN measured by Ding et al. [9]. They found the valence band offset of 1.84 ± 0.1 eV, which means that the conduction bands are at about the same level. From this it is expected that the adding of N to GaAs would mostly affect the electronic properties of the material in the vicinity of the conduction band. Indeed, nitrogen creates energy states to near the conduction band edge and to deep in the valence band [10]. The energy states deep in the valence band do not contribute to the band gap properties of $GaAs_{1-x}N_x$. Thus, the theories describing the alloy concentrate on the conduction band.

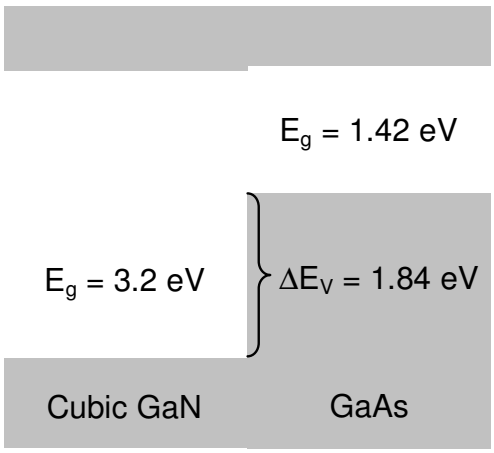

Figure 2. Band offset of GaAs and cubic GaN.

The anomalous properties of $GaAs_{1-x}N_x$ arise from the large size difference between the N and As atoms. The covalent radii of N is 0.068 nm compared to that of 0.121 nm for As. A large difference in the bond length causes lattice relaxation around the substitutional nitrogen atom. This affects the shear deformation potential and thus the valence band splitting of the alloy [11]. The large electronegativity (Pauling scale) of N (3.04) compared to Ga (1.81) and As (2.18) makes the Ga–N bond more polar than the Ga–As bond and favors the electron localization around the N atom.

The large difference between the As and N atoms creates anomalous electrical and optical properties. However, the lattice constant a_o and elastic properties have a linear behavior with increasing substitutional N content of

$GaAs_{1-x}N_x$ [12, 13]. This enables the determination of N composition x with a conventional x-ray diffraction method.

2.2 Impurity and alloy limits

Before Weyers et al. [2] introduced $GaAs_{1-x}N_x$ with x up to 0.016, the common belief was that it is not possible to grow $GaAs_{1-x}N_x$ alloy due to the miscibility gap. The thermodynamical calculations by Stringfellow and Horn [14, 15] showed that the maximum solubility of nitrogen in GaAs would be very low (~ 10^{14} cm^{-3}). Liu et al. [6, 7] achieved N concentrations of over 10^{17} cm^{-3}, which showed experimentally that the thermodynamical solubility limit is possible to be exceeded. The works done by Qiu et al. [16] and Bi and Tu [17] hold the current records for the highest N composition x of single phase $GaAs_{1-x}N_x$ on GaAs and on GaP, respectively. Qiu et al. achieved N composition x = 0.10, which corresponds to the N atom concentration of 2×10^{21} cm^{-3}. Bi and Tu achieved N composition x = 0.148 on GaP, which offers an almost lattice matched substrate for $GaAs_{1-x}N_x$ with this composition. Schlenker et al. [18] showed that the N solubility is dependent on the strain caused by the lattice constant mismatch between the layer and the substrate. According to their calculations the N solubility of GaAsN should be larger on a GaP substrate than on a GaAs substrate. First-principles total-energy calculations by Zhang et al. [19] showed that in the epitaxial growth the maximum solubility is about 8 orders of magnitude larger than the thermodynamic solubility. They found that the maximum N composition x would be about 0.04 at the temperature of 650°C, which is in agreement with the experiments at that temperature. However, higher N compositions are achieved at lower temperatures.

An impurity limit is understood as a composition range, where sharp excitonic transitions are dominating the luminescence spectrum of $GaAs_{1-x}N_x$ at low temperatures. The localized energy state formed by a single N atom is located at 150–180 meV above the conduction band minimum [5, 6] and does not give luminescence at atmospheric pressure. The excitonic luminescence originates from the nitrogen cluster states below the conduction band minimum (CBM). Thus, the composition range of the impurity limit is dependent on the clustering of the N atoms, which, again, is dependent on the growth conditions of the $GaAs_{1-x}N_x$ layer. A typical impurity limit is determined as the composition range of $x < 0.003$ [20].

In the impurity limit, several N-induced localized states are observed [6, 20]. Under hydrostatic pressure, the N related states shift below the CBM and can be detected by photoluminescence measurement. This is because the CBM increases in energy much faster than the localized states as a function of pressure. Usually the impurity states near the CBM shift along with the CBM as

a function of pressure, since their wave functions are constructed mostly from the conduction band. In the case of the strongly localized N state, the wave function is constructed from many bands of the host crystal and thus experiences much smaller pressure coefficient [21]. The N cluster states are formed by N–N pairs with a different distance in the lattice and by clusters having three or more N atoms involved. The energies of the specific cluster states are constant when increasing the N composition x [22], which indicates that the clusters do not interact with each other. As the N composition x is increased, the CBM decreases and overtakes the cluster states below the CBM one by one. The alloy limit is achieved when the CBM is the lowest energy state and the sharp excitonic transitions have disappeared from the luminescence spectrum.

In the alloy limit, the optical properties of $GaAs_{1-x}N_x$ are dominated by the properties of the CBM. However, the local nature of the electronic transitions remains at low temperatures due to local fluctuations of the N composition, which leads to band gap fluctuations and to exciton localization [23, 24]. The localization results in an energy separation between the absorption and the photoluminescence emission of $GaAs_{1-x}N_x$ at low temperatures [22, 25]. A state filling effect also arises from the exciton localization. The photoluminescence peak shifts toward higher energies with increasing number of excited carriers due to the filling of the localized states [23, 24, 26].

The composition dependent bowing of the $GaAs_{1-x}N_x$ band gap results in a strong decrease of the transition energy as N composition x is increased [10, 17]. Recently, Tisch et al. [27] made a careful study on bowing in $GaAs_{1-x}N_x$ using optical transmission measurements at room temperature. The bowing parameter was found to be as large as 40 eV for very low N concentrations ($x < 0.001$) and a constant of about 7.5 eV for high N concentrations ($x > 0.08$). They used the equation

$$b(x) = b_0 + b_1 e^{-x/x_1} + b_2 e^{-x/x_2} \qquad (2)$$

to describe the bowing parameter that fits to their experimental data accurately. They found the following values by fitting: $b_0 = 7.5$ eV, $b_1 = 21.1$ eV, $b_2 = 15.9$ eV, $x_1 = 0.26\%$, and $x_2 = 3.3\%$. The solid line in figure 3 shows the band gap bowing given by equation 2. The dashed line in figure 3 shows an estimated band gap at the temperature of 10 K based on the room temperature data and on the decreasing band gap temperature dependence with increasing N composition x [28, 29].

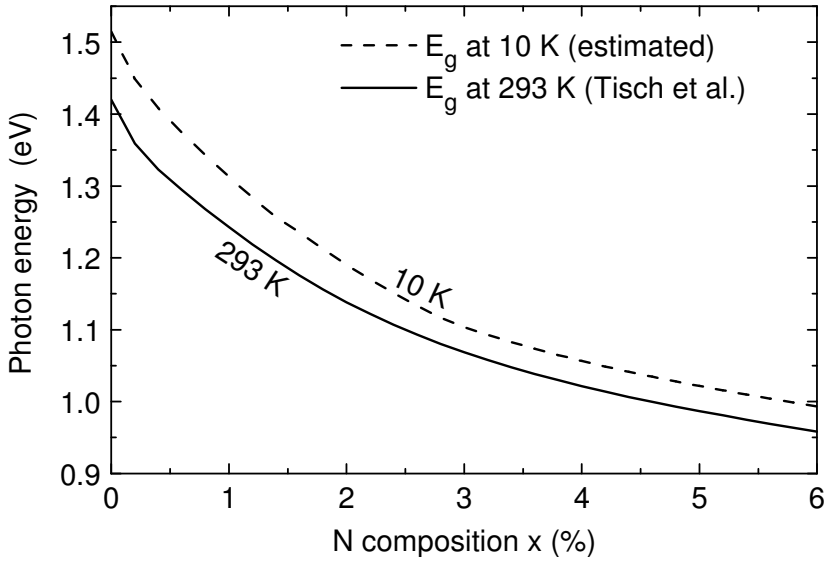

Figure 3. Band gap energy as a function of N composition x in $GaAs_{1-x}N_x$.

The electron effective mass in the $GaAs_{1-x}N_x$ conduction band increases when nitrogen is introduced to the layer [30]. However, the value of the effective mass as a function of N concentration is not clear. Zhang et al. [31] found that the effective mass increases rapidly with N composition x and then gradually decreases as the N concentration increases further ($x > 0.01$). Hai et al. [32] reported effective mass values of 0.12 m_o and 0.19 m_o with the N compositions of 1.2% and 2.0%, respectively. Their report suggests that the effective mass will continuously increase with increasing N composition x. The gradually increasing electron effective mass as a function of the N concentration has obtained further support recently [33].

A new energy band in $GaAs_{1-x}N_x$ was observed above the conduction band minimum [34, 35]. It appears at above the single N atom resonant state in energy and is denoted as E_+ state. The E_+ state shifts toward higher energies linearly with increasing N composition. It shifts with a similar rate as the conduction band minimum (denoted as E_) shifts toward lower energies. The appearance of this new band has been explained in two different ways: with the band anticrossing model and with the pseudopotential theory, which are explained in the following sections.

2.3 Band anticrossing model

The band anticrossing (BAC) model was introduced by Shan et al. [34] to describe the observed two-level repulsion [35] in the GaInNAs alloy. The band anticrossing model explains the pressure and composition dependencies of the

$GaAs_{1-x}N_x$ alloy by conduction band splitting. The splitting is caused by N-induced perturbation, which is enhanced as the N concentration increases. The new conduction bands are denoted as E_- and E_+, and the energy difference between them increases with increasing N concentration. The BAC model was used successfully to predict an increase in the electron effective mass in GaInNAs alloys [30]. Despite the oversimplified physical picture, the model has been shown to describe the material properties of Ga(In)NAs very well [36–39].

Figure 4(a) shows the anticrossing behavior between the localized state of nitrogen and the conduction band of GaAs. The N-induced energy state E_N is spread over the reciprocal space with constant energy due to the localized nature of N-induced electron state. The energy state E_N and the energy dispersion of GaAs conduction band $E_M(k)$ are drawn with dashed lines. As a result of the anticrossing interaction, the energy bands E_- and E_+ are formed. The band anticrossing model explains only the conduction band splitting, and the valence band is assumed to be unaffected by nitrogen.

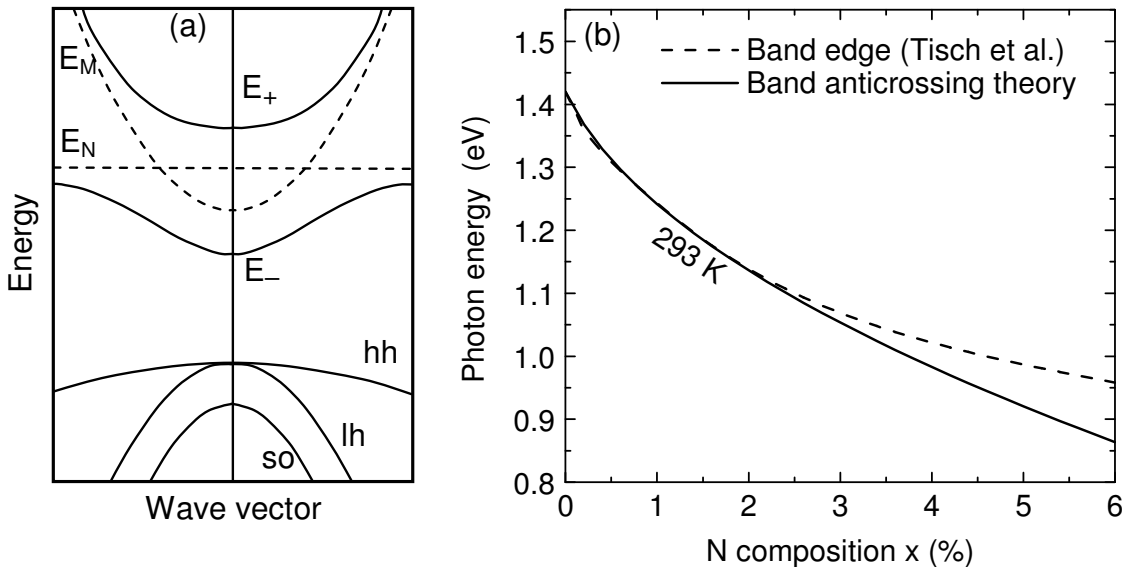

Figure 4. (a) Schematic illustration of band anticrossing model of $GaAs_{1-x}N_x$. (b) Band gap energy of $GaAs_{1-x}N_x$ as a function of N composition x.

An advantage of the BAC model is that it provides simple analytic expressions for the conduction band dispersion and for the electron effective mass as a function of N composition x. The new bands, E_- and E_+, can be expressed as [40]

$$E_{\pm}(k) = \frac{1}{2}\left(E_N + E_M(k) \pm \sqrt{\left(E_N - E_M(k)\right)^2 + 4C_{NM}^2 \cdot x} \right), \qquad (3)$$

where E_N is the energy of localized nitrogen state, $E_M(k)$ is the dispersion of the host crystal (GaAs) conduction band, C_{NM} is a constant describing the strength of the anticrossing interaction, and x is the N composition. All the energies are relative to the valence band maximum of the unperturbed host crystal. Figure 4(b) shows with a solid line the band gap of $GaAs_{1-x}N_x$ as a function of N composition calculated with equation 3. Values used for E_N and C_{NM} were 1.65 eV and 2.7 eV, respectively. A value of $E_M(0) = 1.42$ eV was used for the GaAs band gap. The dashed line in figure 4(b) shows the measured band gap of $GaAs_{1-x}N_x$ by Tisch et al. [27]. The BAC model gives an excellent fit when the N composition x is smaller than 0.03. With a larger x, there is a significant discrepancy between the experimental band gap and the BAC model. The BAC model predicts that the band gap will close at $x \approx 0.3$, whereas the experimentally determined band gap seems to have a minimum value of 0.3 eV at $x \approx 0.4$ [27]. The suitable N composition range for the BAC model is not clear, but it seems to work fine at least with $x < 0.03$.

The BAC model gives a simple analytic expression for the electron effective mass. Using equation 3, the effective mass is derived as [30]

$$\frac{1}{m^*} = \frac{1}{\hbar^2 k}\left|\frac{\partial E_-(k)}{\partial k}\right|_{k=0} = \frac{1}{2m_M}\left[1 - \frac{E_M(0) - E_N}{\sqrt{\left(E_M(0) - E_N\right)^2 + 4xC_{NM}^2}}\right], \quad (4)$$

where m_M is the electron effective mass in the host crystal. Equation 4 can be simplified to the form

$$m^* = m_M\left(1 + \frac{xC_{NM}^2}{\left(E_N - E_-\right)^2}\right). \quad (5)$$

Figure 5 shows the electron effective mass of $GaAs_{1-x}N_x$ calculated with equation 5. The model predicts that the effective mass will increase rapidly to about 0.1 m_o when x = 0.01 and then saturates to the value of about 0.11 m_o with larger x. It is not obvious that the prediction for the effective mass is correct, even if the prediction for the band gap is very good. However, the majority of the experimental works support the BAC model prediction about the non-parabolic conduction band and the increased electron effective mass in $GaAs_{1-x}N_x$ [30, 32, 33].

Table 1 shows the typical values used to describe the properties Ga(In)NAs band gap with the BAC model [41]. The values for C_{NM} and E_N are well established and the band gap of the host crystal ($In_yGa_{1-y}As$) is used as $E_M(0)$. Table 1 gives an estimate for the band gap of $In_yGa_{1-y}As$ in various conditions.

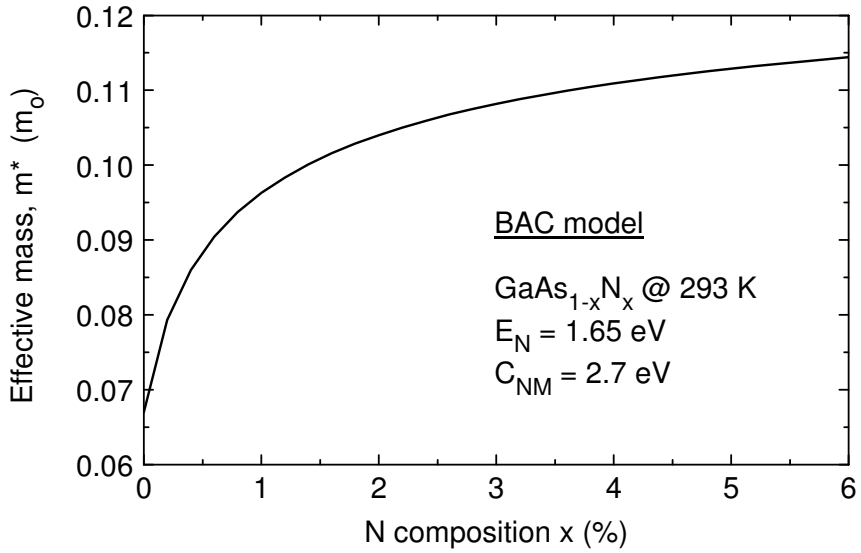

Figure 5. Electron effective mass in $GaAs_{1-x}N_x$ calculated with band anticrossing model.

The band anticrossing model motivated the development of a 10-band **k·p** method [42, 43]. A **k·p** theory describes the dispersion of the bands very accurately with a small wavevector **k**, typically when $|\mathbf{k}| < 0.2\ k_{max}$, where k_{max} is the maximum wavevector in the first Brillouin zone. The **k·p** method is widely applied to study III–V semiconductor quantum well structures and alloys. A 6-band **k·p** method describes the coupling between twice spin-degenerated light-hole, heavy-hole and split-off bands by means of the Luttinger Hamiltonian. An 8-band **k·p** method includes the coupling between the valence bands and the spin-degenerated conduction band. The coupling depends on the bulk dipole matrix element and the wavevector **k**. In the 10-band **k·p** method, the interaction between spin-degenerated N-induced defect level and the conduction band is included by means of the BAC model. The 10-band **k·p** method gives an accurate description of the dispersion of the bands in the Ga(In)NAs alloy and quantum wells. Due to the strong non-parabolic nature of the bands in Ga(In)NAs, quantum well energy states can not be calculated using the conventional technique that assumes parabolic bands [39]. The 10-band **k·p** method has been shown to accurately describe the energy states in GaAsN quantum wells and a valence band offset of (30 ± 15)% was found to give the best fit to data [44]. The method was successfully used to model optical gain in GaInNAs laser structures [38, 45, 46].

Table 1. Parameters for band anticrossing model to calculate conduction band properties of Ga(In)NAs [41].

C_{NM}	2.7 (eV)
E_N (300K)	1.65 (eV)
dE_N/dp	0.015 (eV Gpa^{-1})
dE_N/dT	-0.00025 (eV K^{-1})
dE_M/dp	0.105 (eV Gpa^{-1})
$E_g(In_yGa_{1-y}As)_{T=0K}$	$1.512 - 1.337\ y + 0.27\ y^2$ (eV)
$E_{g,InGaAs}(T)$	$E_{g,InGaAs} - \alpha T^2 / (\beta + T)$
	$\alpha = 5.408 \times 10^4$ (eV K^{-1}), $\beta = 204$ (K)

2.4 Pseudopotential method

The pseudopotential method is a microscopic theoretical model used to calculate wavefunctions and band energies of semiconductors. In the empirical pseudopotential method (EPM), experimentally corrected pseudopotentials are used and thus the method can generate accurate energies for the electron states [47]. The method was used to predict the composition dependent bowing and localization of electron states in GaAsN [10]. The EPM uses a periodically repeated supercell to describe the atomic structure of the system under investigation. The method enables a supercell size of up to 10^4 atoms, which makes it suitable to use also in impurity, cluster and atomic ordering studies. To calculate the effect of atomic relaxation in EPM, an independent technique has to be used to obtain the new atomic positions. The relaxed atomic positions can be obtained for example by a valence force field method (VFF) [48], which treat atoms and bonds like balls and springs, respectively. The relaxation of Ga atoms around the N atom in GaAsN has been shown to have a strong effect on conduction band mixing and thus to cause the strong bowing of the conduction band edge [49, 50].

The main difference between the band anticrossing model and the empirical pseudopotential method is in the origin of the E_+ band. In the BAC model the E_+ band is formed due to the anticrossing of the GaAs conduction band and the localized N state, while in EPM the E_- and the E_+ bands originate from the mixing of $a_1(\Gamma)$, $a_1(L)$ and $a_1(X)$ states with a negligible contribution of the N state. Figure 6(a) shows a schematic illustration of the EPM calculation results in the N composition x range of about 0–0.01 [51]. Mattila et al. [51] have shown that the energy of the N state increases rapidly as a function of the N concentration and would not be constant as assumed in the BAC model. They

also found that the E_ energy state is formed by hybridization of $a_1(\Gamma)$ and $a_1(L)$ states and that it is not sensitive to the configuration of N atoms in the supercell. The Γ content of the E_ band was found to decrease as a function of the N composition, whereas the Γ content of $a_1(L)$ was found to increase. The optical transition probability between the valence band minimum and the conduction bands was found to be directly proportional to the percentage of the Γ character in the conduction bands. Mattila et al. suggested that the E_+ band would originate from a configuration weighted average of the $a_1(N)$ and $a_1(L)$ levels. Recently, Gorczyca et. al [52] stated that the observed E_+ transition would actually be the transition between the $a_1(L)$ and valence band maximum levels.

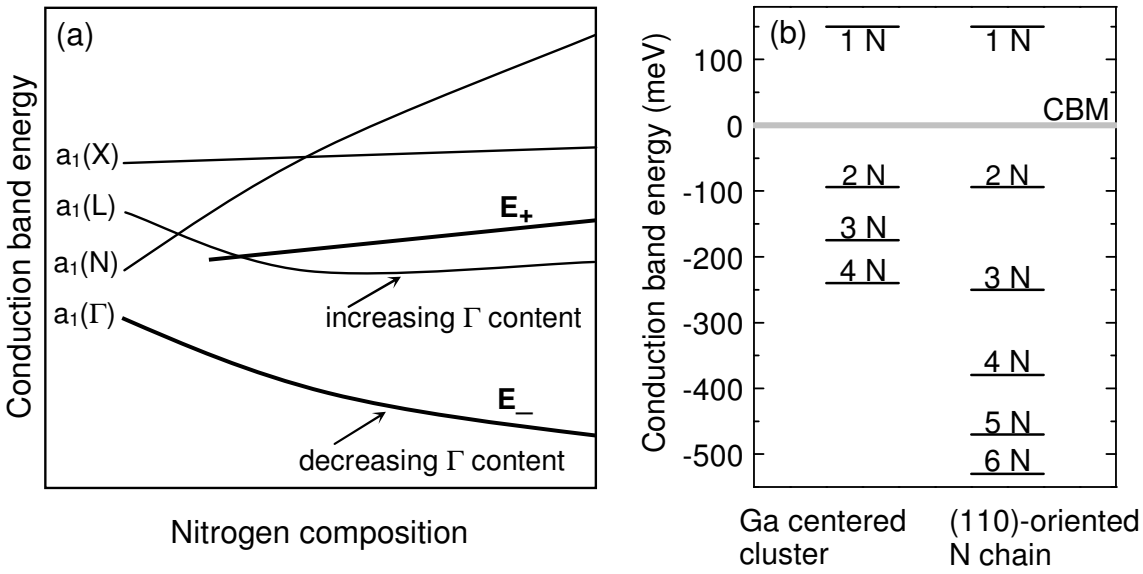

Figure 6. (a) Schematic illustration of GaAsN conduction bands in pseudopotential theory as a function of N composition [51]. (b) Energies of N cluster states in GaAs calculated with pseudopotential theory [50].

Figure 6(b) shows the calculated energy levels of the N clusters in GaAs [50]. Two different cluster configurations were found to form energy states in the band gap. The first one is a cluster where a Ga atom is surrounded by a number of N atoms. A band gap state is formed with 2–4 N atoms. The second configuration is a (110)-oriented chain of N atoms. The number of N atoms is not limited and the energy state of the cluster lowers as the number of N atoms in the chain increases.

3 EPITAXIAL GROWTH

The arsenide-nitride materials studied in this thesis are grown on GaAs substrates using metalorganic vapor phase epitaxy (MOVPE). An exception is publication II, which is a study on samples prepared by molecular beam epitaxy (MBE). MOVPE and MBE are methods to grow epitaxial layers on a substrate crystal. Section 3.1 describes the MOVPE technique that has been in the focus of this thesis. In the following sections the MOVPE growth of arsenide-nitrides is discussed and selected experimental results from publications are presented. Section 3.2 introduces the commonly used precursors. The effect of growth parameters like growth temperature, growth rate, V/III-ratio, and growth pressure and carrier gas are discussed in sections 3.3, 3.4, 3.5, and 3.6, respectively. Section 3.7 compares the properties of the two different growth methods.

3.1 Metalorganic vapor phase epitaxy

In the MOVPE process a stable flow of metal organic source materials in a carrier gas is conducted over a heated substrate in a reactor. The epitaxial growth takes place when the metal organic precursor molecules decompose in the hot zone over the substrate and the group-III and the group-V elements diffuse to the surface of the substrate. After the adsorption of atoms to the surface, they can diffuse on the surface, nucleate into the growing epilayer or desorb away. Some precursors do not decompose until they reach the surface. Due to different properties of source materials, it is crucial to find a proper temperature, pressure and combination of precursors to grow high quality crystal.

The synonyms used for MOVPE are metalorganic chemical vapor deposition (MOCVD), OMVPE and OMCVD. The development of the MOVPE technique has begun at the end of the 1960's [53]. Nowadays, MOVPE machines are capable of producing atomically sharp heterointerfaces with an excellent uniformity over a number of wafers. The largest reactors can handle 95 2-inch wafers at a time. The increase of reactor size and the enhancement of growth uniformity are the results of temperature and flow dynamics modeling. One of the newest development steps of MOVPE machines is an optical in-situ monitoring of the growing layer [54]. Optical techniques enable accurate surface temperature, growth rate and doping level measurements, which can be utilized to achieve a more precise growth control.

The epitaxial Ga(In)NAs layers studied in this thesis were grown at Optoelectronics Laboratory in Helsinki University of Technology. The MOVPE machine was manufactured by Thomas Swan Scientific Equipment Ltd. and it was installed in 1993. It has a horizontal quartz tube reactor with a cross-sectional area of 5 cm^2. Figure 7 shows the schematic view of the machine. The vent line was purged with nitrogen and purified hydrogen was used as a carrier gas elsewhere. Hydrogen was purified with a passive purifier that effectively removes all the impurities containing oxygen. Precursors are located in bubblers, which are held in baths at a stabilized temperature. Mass flow controllers (MFC) are used to control the flow of the carrier gas through the liquid source materials in the bubblers, where the carrier gas is saturated with the metal organic precursors. The temperatures of the baths are used to control the concentration of the precursors in the carrier gas due to temperature dependent vapor pressures of the precursors. Prior to the growth, the precursors in the carrier gas are directed to the vent line to stabilize the flow rates and the concentrations. The vent line is directed through the pyrolysis furnace to the exhaust. To initiate the growth the proper precursors are directed to the reactor. After the reactor the gas flow is directed to the exhaust. At exhaust the metal organics, by-products and desorbed elements are absorbed and oxidized in a charcoal scrubber.

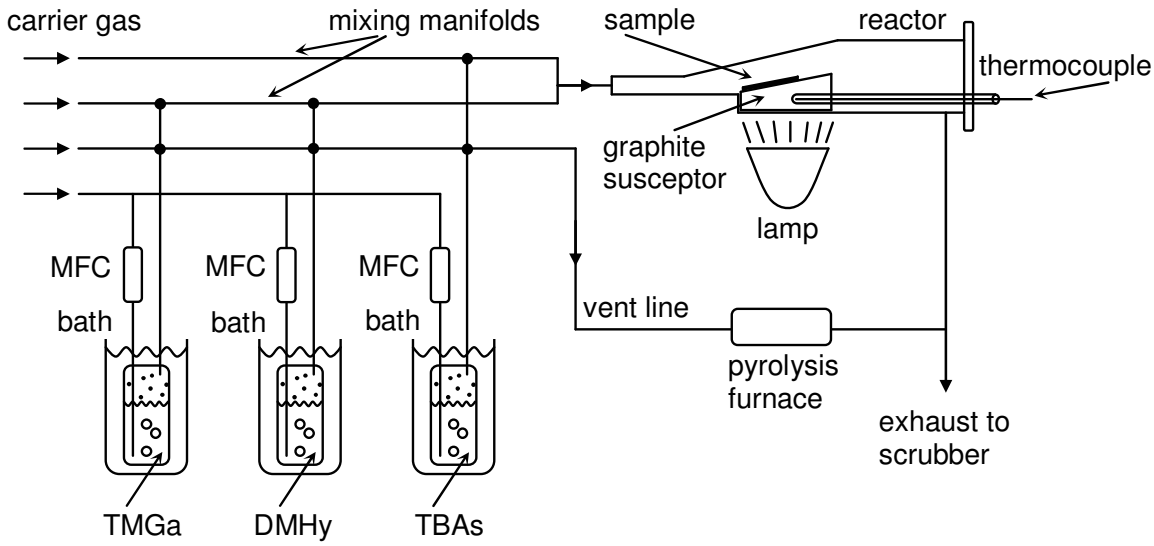

Figure 7. Schematic illustration of MOVPE machine.

The precursors used to grow Ga(In)NAs were trimethylgallium (TMGa), trimethylindium (TMIn), dimethylhydrazine (DMHy) and tertiarybutylarsine (TBAs). Separate mixing manifolds are used for the group-III and the group-V source materials to prevent unwanted reactions before the reactor. However, DMHy is injected to the group-III mixing manifold due to the lack of a proper connection to the group-V manifold. The time for the pre-reactions is still very

short, because of the high carrier gas flow (5.5 liters per minute). Usually metalorganics are in liquid form at room temperature, but an exception is TMIn that is solid (not shown in figure 7). However, we have used a liquid solution TMIn precursor, where solid TMIn is suspended in an extremely low vapor pressure adduct solution N,N-Dimethyldodecylamine [$(CH_3)_2NC_{12}H_{25}$]. The evaporated TMIn is continuously replenished by dissolution during the usage. The advantages of solution TMIn are a constant output of TMIn over the entire life of the source, a speedy response like other liquid metal organics and effectively the same vapor pressure as solid TMIn.

A halogen lamp heats the susceptor in the reactor and the temperature is controlled by a thermocouple located inside the susceptor. All the growth temperatures mentioned in this thesis are thermocouple readings. Because of the cooling effect of the flowing gas, the actual surface temperature of the substrate is lower than the controlled susceptor temperature. For a similar reactor, the surface temperature of the substrate has been measured to be about 50°C lower than the thermocouple reading at the nominal temperature of 650°C [55]. All the growth processes were conducted under the atmospheric pressure.

3.2 Precursors

GaAsN is a relatively new material, and the most suitable combination of precursors for the MOVPE-growth is not yet clear. A low growth temperature of 500°C–600°C is needed for the N incorporation. Therefore, precursors with low decomposition temperatures are needed. The concentrations of background impurities, like carbon, hydrogen and oxygen, increase at low growth temperatures. Thus, it is important to choose precursors, which are known to generate low background impurity concentrations and are as pure as possible.

Tertiarybutylarsine [$(CH_3)_3CAsH_2$] (TBAs) was used as a precursor for arsenic in this thesis. The most common source for arsenic in MOVPE is arsine (AsH_3), which is gaseous. However, arsine is very toxic. TBAs is liquid at room temperature, which makes it much more convenient to handle. In addition to safety issues, TBAs has been shown to have advantages over arsine when growing at low temperatures [56]. This is mainly due to the about 200°C lower decomposition temperature of TBAs than that of arsine [57].

Trimethylgallium [$(CH_3)_3Ga$] (TMGa) was used as a precursor for gallium in this thesis. Another typical source for gallium in MOVPE is triethylgallium [$(C_2H_5)_3Ga$] (TEGa). Both precursors are liquid at room temperature and have similar properties in MOVPE-growth. TMGa [58] and TEGa [59–61] have been suggested to form adducts in gas phase with dimethylhydrazine, which is commonly used as a nitrogen source. TMGa and TEGa differ in their decomposition temperature and in their by-products. TMGa decomposes

incompletely at low temperatures, and thus the growth rate decreases when the temperature is decreased. TEGa has a lower decomposition temperature and provides a constant growth rate at temperatures from 700°C down to 500°C [62]. The unintentional C-doping is greatly enhanced at low growth temperatures when using TMGa as a gallium source [63]. This is due to a stable monomethylgallium molecule and is avoided by using TEGa as a gallium source. The by-products of the precursors might have a significant role in MOVPE-growth. TMGa produces reactive CH_3 radicals, which might affect the N incorporation by forming methylamine with NH_2 radicals [62, 64]. Overall, TEGa is considered a more suitable source of Ga for low-temperature-grown arsenide-nitrides than TMGa [65].

Several precursors have been used to incorporate N to arsenide-nitrides. Ammonia (NH_3) is a common precursor for III-N materials grown at high temperatures and the first GaAsN alloys were grown with precracked ammonia [2, 8]. Ammonia has also been used for (Al)GaAsN without precracking [66]. In MBE-growth precracked nitrogen gas (N_2) is a widely used N source [67, 68]. Other precursors that are successfully used for metalorganic MBE and MOVPE of arsenide-nitrides are 1,1-dimethylhydrazine (DMHy) [69, 70], monomethylhydrazine [71], hydrazine [62], tertiarybutylhydrazine (TBHy) [72, 64] and nitrogen trifluoride (NF_3) [62]. Figure 8 illustrates some of the N precursor molecules. A common feature of hydrazine-type precursors is that they all release NH_2 radicals when they decompose. The most widely used N source for MOVPE of arsenide-nitrides is DMHy, even though it shows a very low N incorporation efficiency. Bourret-Courchesne et al. [61] reported that the decomposition of DMHy starts at 320°C and is fully decomposed at 800°C. They found that the pyrolysis of DMHy begins with the cleavage of N–N bond and that also the $(CH_3)_2N$-radical decomposes at temperatures higher than 515°C. The large amount of different radicals in the gas phase leads to complicated reactions and thus the properties of the crystal growth might vary

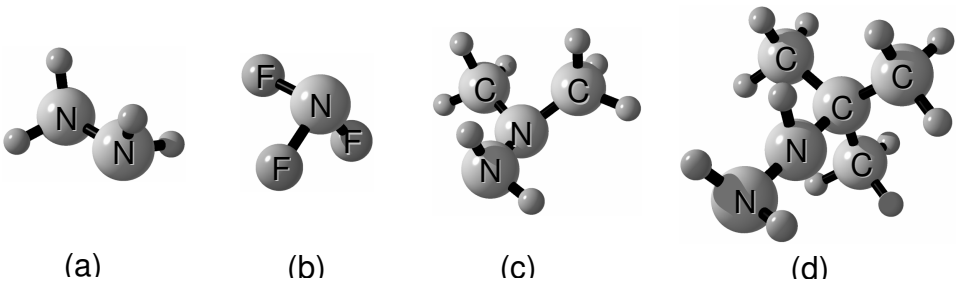

Figure 8. Precursor molecules for nitrogen in arsenide-nitrides:(a) hydrazine, (b) nitrogen trifluoride, (c) 1,1-dimethylhydrazine (DMHy) and (d) tertiarybutylhydrazine (TBHy). Small atoms without labels are hydrogen atoms.

largely between different types of reactors. NF_3 was recently shown to be the most effective N source for arsenide-nitrides [64].

In publication I, the growth of $GaAs_{1-x}N_x$ using DMHy as a source of N was studied. Figure 9 shows the dependence of the N composition x on DMHy/V ratio, where V = TBAs + DMHy. The N composition was determined using x-ray diffraction method. In this set of samples the TBAs flux was kept constant at a value of two times the TMGa flux, which was fixed to obtain a growth rate of 1.1 μm/h. The growth temperature was 530°C. A distribution coefficient k_N for N over As is determined as

$$k_N = \frac{X_N / X_{As}}{F_{DMHy} / F_{TBAs}}, \tag{6}$$

where X_N and X_{As} are the solid compositions of nitrogen and arsenic. F_{DMHy} and F_{TBAs} are the molar fluxes of the precursors in the gas phase. A very low distribution coefficient of 0.0052 was found for nitrogen even in these optimized growth conditions for N incorporation. In addition to the low incorporation efficiency, saturation of the N composition was observed with DMHy/V ratios larger than 0.92. However, a composition of $0 < x < 0.056$ for $GaAs_{1-x}N_x$ was achieved with DMHy. It was used as a N source also for the subsequent studies on properties of $GaAs_{1-x}N_x$ in this thesis.

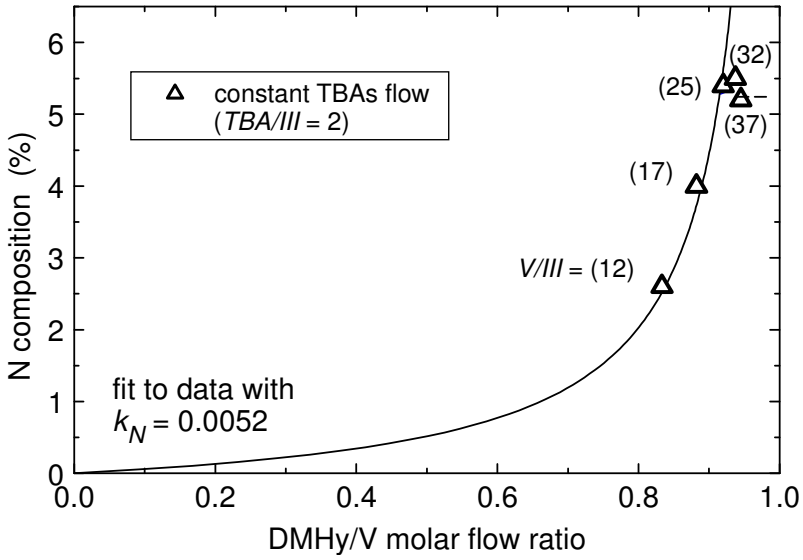

Figure 9. N composition x of $GaAs_{1-x}N_x$ as a function of DMHy/V ratio [Publ. I].

3.3 Temperature

The growth temperature is probably the most important parameter in controlling the epitaxial growth of arsenide-nitrides. The growth temperature has

influence over the rates of all the chemical reactions and over kinetics of the molecules and atoms in gas phase and on the surface. Arsenide-nitrides have been grown with MOVPE at temperatures from 475°C to 700°C [62, 69, 73]. The N composition x decreases rapidly with increasing growth temperature [69], which is probably caused by the temperature enhanced N desorption from the surface [74]. Thus, a low growth temperature of less than 550°C has to be used to incorporate enough N for the aimed 1.3 μm emission. An advantage of the low growth temperature is a small enhancement in the critical thickness [75]. It allows the growth of thicker strained quantum wells, which appears as reduced photon energy. Drawbacks of the low growth temperature are the increased impurity concentrations [63, 76] and the deteriorated material properties of arsenide-nitrides [69, 73]. Thus, the determination of the growth temperature is a compromise between the N incorporation efficiency and the material quality.

In publication IV, the effect of the growth temperature on the N composition of $Ga_{1-y}In_yN_xAs_{1-x}$ was studied. Two In compositions of y = 0.1 and y = 0.3 were used. Figure 10 shows the rapid decrease of the N composition with increasing growth temperature. The effect is even more pronounced with a larger In concentration. Increase in the In composition results in a decrease of the N composition. The process causing the effect is still unclear, but the increase in the growth temperature seems to speed it up. Decreasing the growth temperature below 520°C results in poor crystal quality. Thus, the optimum growth temperature for N incorporation was found to be 520°C. The properties of $Ga_{1-y}In_yN_xAs_{1-x}$ are discussed further in the chapter 6.

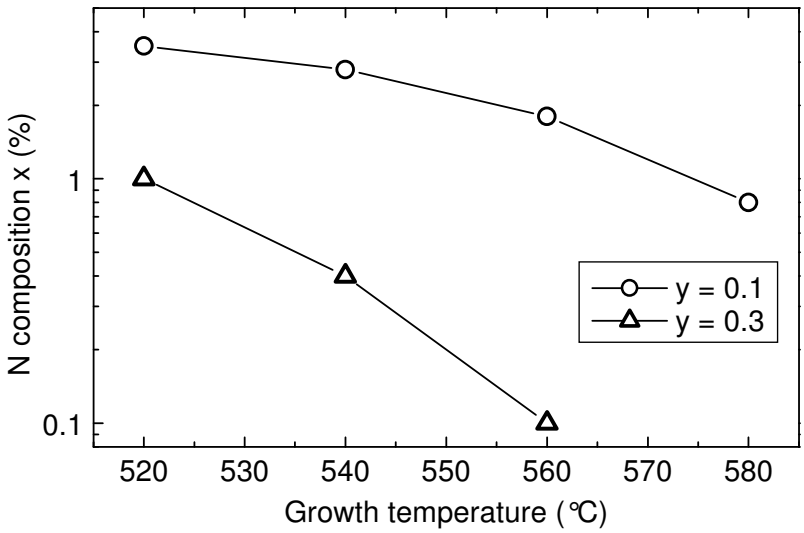

Figure 10. N composition x of $Ga_{1-y}In_yN_xAs_{1-x}$ as a function of growth temperature for two In compositions y = 0.1 and y = 0.3 [Publ. IV].

3.4 Growth rate

In the MOVPE-growth of arsenide-nitrides, the N composition has been found to increase with increasing growth rate [62, 77]. This is probably due to the reduced desorption time for N at the surface. However, the high growth rate also shortens the migration lengths of atoms at the surface, which may lead to surface roughening. The best material quality is achieved with a low growth rate of about 0.15 μm/h [73, 78]. Again, here is a compromise between the N incorporation efficiency and the material quality.

The growth rate of crystal is mainly determined by the total flux of group-III precursors. An incomplete TMGa decomposition at low temperatures [62] and prereactions between precursors [59] also have an impact on the growth rate of arsenide nitrides. In publication IV we have estimated a decrease in the growth rate due to the incomplete TMGa decomposition for GaAs and GaAsN by 10% at 540°C and by 15% at 520°C compared to the growth rate at higher temperatures.

3.5 V/III-ratio

An excess of group-V precursors is applied in epitaxial growth of III–V compound semiconductors to protect the crystal surface. The desorption of the group-V atoms from the surface enhances with increasing temperature, whereas that of group-III atoms is assumed to be negligible at the typical range of growth temperatures. Thus, at higher temperatures a larger excess of group-V precursors has to be used.

For the surface protection of $GaAs_{1-x}N_x$ in MOVPE at low growth temperatures a very low TBAs/III ratio of about two is sufficient. The surface of $GaAs_{1-x}N_x$ with a small x is mostly covered by arsenic and the desorption of arsenic is slow at low growth temperatures. The As and N atoms are competing for the same lattice site in the crystal. Thus, the N composition x is effectively controlled by TBAs/III ratio [77] and the N composition increases with decreasing TBAs/III ratio. However, the surface protection is lost if the TBAs/III ratio is decreased below a critical limit and the atomically flat surface changes into three-dimensional features.

In publication I, the optimal growth conditions for the maximum N incorporation were studied. The growth temperature of 530°C and the growth rate of 1.1 μm/h were used. Figure 11 shows the N compositions obtained with different TBAs and DMHy fluxes. The triangles show the effect of increasing DMHy flux, while the TBAs/III ratio was kept constant. The N composition increases almost linearly up to x = 5% with increasing DMHy flux and then saturates to the maximum value of 5.6%. The circles show the effect of the

TBAs flux. The N composition is decreased rapidly, when the TBAs flux is increased. Several attempts were used to achieve a larger N concentration by decreasing the TBAs/III ratio. However, the x-ray diffraction satellite peaks of $GaAs_{1-x}N_x$/GaAs multi quantum well structures disappeared when the TBAs/III ratio was decreased further. Thus, the critical limit for the TBAs/III ratio with used growth parameters was two. The dashed lines in figure 11 connect the data points with the same DMHy/V ratios. They show that the N composition is dependent also on the V/III ratio when the ratio of DMHy and TBAs is kept constant. The dependence of the N composition on the V/III ratio increases with increasing DMHy/V ratio.

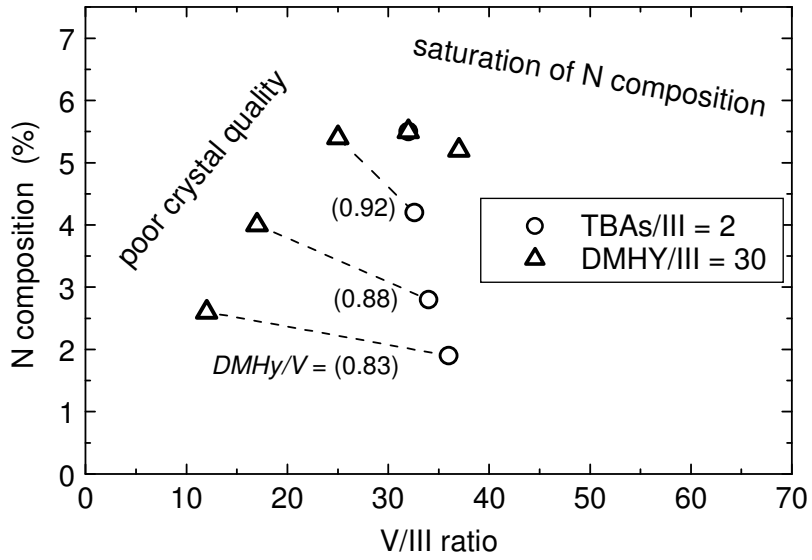

Figure 11. N composition x of $GaAs_{1-x}N_x$ as a function of V/III ratio [Publ. I]. Dashed lines are guides to eye.

The V/III ratio affects the migration length of group-three atoms on the surface. The topmost group-III atoms migrate on the surface, but when they are covered with group-V atoms, the movement is halted. With a high V/III ratio the mean migration length of the surface atoms is decreased. Alexandre et al. [79] found that the optical quality of the arsenide-nitride quantum wells was greatly enhanced with a high V/III ratio. They used a high TBAs/III ratio to stabilize the growth surface and a high DMHy/V ratio to still obtain a sufficient N incorporation.

3.6 Pressure and carrier gas

The reactor pressure and the carrier gas flux are parameters used to control the gas flow dynamics in the reactor. Hydrogen is typically used as a

carrier gas. The aim is a laminar flow of gas without vortices to obtain a uniform growth conditions across the reactor. The suitable pressures and gas flows are reactor-specific. The uniform gas flow is difficult to achieve in atmospheric pressure, and thus low pressures are used to speed up the gas flow and to achieve a vortex free gas flow and uniform growth conditions.

The gas speed and pressure also have an effect on the diffusion of the molecules in the gas phase, the switching speed between the grown materials, and the temperature distribution in the reactor. At low pressures the diffusion is enhanced, which increases the prereactions between the precursors. However, the gas speed is also increased at low pressures and thus the time for the prereactions is shorter than at the atmospheric pressure. By changing the carrier gas from H_2 to N_2 the diffusion is decreased without changing the reaction time in the gas phase [80]. The selection of the carrier gas might have an effect on the reactions in the gas phase also by definition. Hydrogen usually has a role in the reactions of metalorganics. The switching speed is important in the growth of complicated structures like quantum dots and the temperature distribution in the reactor has an effect on the growth uniformity.

Ougazzaden et al. [81] studied the effect of N_2 carrier gas on the growth of arsenide-nitrides. They found that the N incorporation efficiency was increased and that the interaction between In and N incorporation was decreased when using N_2 as a carrier gas. The mechanism behind the phenomenon is not clear. However, the carrier gas mixture of H_2 and N_2 gives a new independent parameter for the growth control of arsenide-nitrides. A large H impurity concentration has been observed in arsenide-nitrides grown by MOVPE [76]. Kurtz et al. [63] reported that the change of the carrier gas from H_2 to N_2 has no effect on the H impurity concentration in the solid. Thus, the large H concentration originates from the precursor molecules.

3.7 MOVPE vs. MBE

The molecular beam epitaxy (MBE) differs in many ways from MOVPE in the growth of arsenide-nitrides, especially when elemental solid sources are used in MBE. The MBE-growth is performed in a vacuum and the atomic In, Ga and As are evaporated from their solid counterparts. The atomic N is cracked from N_2 gas with a radio-frequency plasma cell. Thus, pure reactive atomic sources are delivered to the MBE chamber. In such conditions, much lower growth temperatures can be used and, overall, the growth is easier to control. The decomposition of precursors, the prereactions between them and the concentration of background impurities are not a concern. However, MOVPE has advantages over MBE in production related issues like easy maintenance, high uptime, good growth uniformity, and lower total expenses. And after a

careful optimization of growth conditions, the difference in the resulted material quality is typically small between these growth methods [4]. However, some defects related material properties of MOVPE- and MBE-grown arsenide-nitrides are found to be different [82]. Thus, the growth method should be noticed when studying the material properties of arsenide-nitrides.

4 STRUCTURAL PROPERTIES

The structural properties of $GaAs_{1-x}N_x$ were studied in this thesis using several experimental methods. The surface morphology of the material is discussed in section 4.1 by means of the atomic force microscopy results. Section 4.2 describes the use of x-ray methods in the dislocation formation studies and in the determination of the critical thickness of $GaAs_{1-x}N_x$ on GaAs. Section 4.3 introduces the point defects found in $GaAs_{1-x}N_x$ and section 4.4 describes the study of gallium vacancies using positron annihilation spectroscopy.

4.1 Surface morphology

The surface morphology of arsenide-nitrides has been found to change from an atomically flat surface into three-dimensional structures when the N composition is increased [77, 83, 84]. The low growth temperature, that is required for the N incorporation, prevents the step-flow growth of the material. In the two-dimensional step-flow growth, the atoms migrate on the surface until they reach atomic steps and the growth occurs only at those steps. Thus, the surface is constantly as flat as possible and the heterointerfaces between the materials are possible in the scale of one monolayer. At low growth temperatures the migration length is decreased. When the mean migration length is smaller than the distance between atomic steps, the growth mode is changed to quasi-two-dimensional. The growth occurs at one-monolayer-high islands, which are randomly distributed at the surface. This growth mode is typically detected for arsenide-nitrides [77], and the surface roughness has been found to increase with increasing N composition [83]. For the N composition x over 0.04 also three-dimensional surface structures are detected [77, 83]. The possible reasons for the three-dimensional structures at high N compositions are an insufficient arsenic protection of the surface and the high strain between the substrate and the epilayer.

In publication VI, the surface morphology of $GaAs_{1-x}N_x$ on GaAs was studied with atomic force microscopy (AFM). In AFM the surface is scanned with an extremely sharp tip using piezo actuators, and the height of the tip is measured with a laser beam reflection. The technique provides an atomic resolution in the vertical direction and a resolution of 10–50 nm in the horizontal plane depending on the tip. Figure 12 shows two AFM images recorded with a silicon nitride tip in the contact mode. Figures 12(a) and 12(b) show the surfaces

of $GaAs_{0.965}N_{0.035}$ layers before and after annealing, respectively. The roughness of the as-grown surface is more than one monolayer. The height range is 0.57 nm, which corresponds to about two monolayers. This is the typical roughness that was obtained with N compositions from 0 to 0.056. Due to annealing at 700°C the surface was smoothed. The height range in the figure 12(b) is 0.27 nm, which corresponds to about one monolayer. The atomic steps are clearly seen. The three-dimensional surface structures were not observed even at N compositions over 0.04. The only indication of the interface degradation between $GaAs_{1-x}N_x$ and GaAs was found in publication I. The x-ray diffraction satellite peaks of the $GaAs_{1-x}N_x$/GaAs multi quantum wells disappeared, when the TBAs/III ratio was decreased below two. Similar behavior was reported in the Ref. 77. However, we have shown that the $GaAs_{1-x}N_x$ with the N composition x of up to 0.056 can be grown without a significant surface degradation as long as the surface protection with arsenic is sufficient.

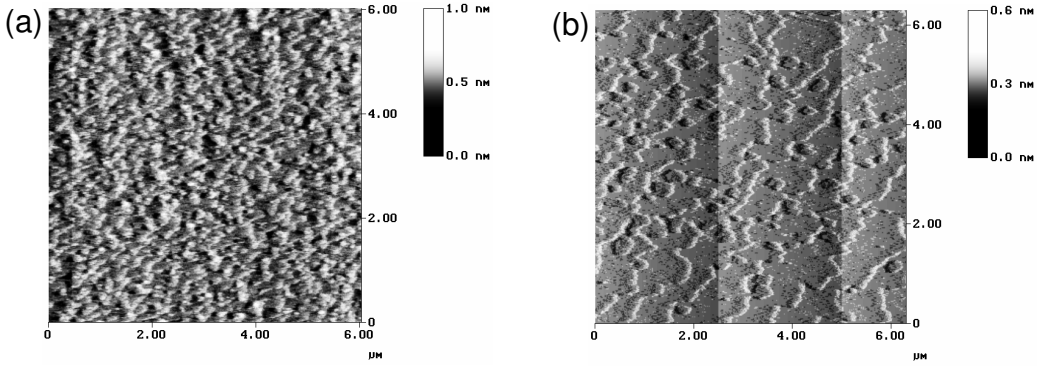

Figure 12. Atomic force micrographs of (a) as-grown and (b) annealed 130-nm-thick $GaAs_{0.965}N_{0.035}$ layers on GaAs.

4.2 Misfit dislocations

A critical thickness in the heteroepitaxial growth is understood as the thickness that can be grown coherently without a formation of misfit dislocations or three-dimensional islands. The lattice constant of the coherently grown epilayer is strained to that of the substrate in the horizontal plane. The critical thickness decreases with increasing lattice mismatch between the epilayer and the substrate. When the epilayer is thicker than the critical thickness, the strain relaxes through the misfit dislocations or the island formation. Thus, it is important to know the critical thickness of the material system to be able to grow high quality strained $GaAs_{1-x}N_x$ epilayers on GaAs.

Uesugi et al. [85, 86] studied the critical thickness of $GaAs_{1-x}N_x$ on GaAs with different N compositions using a high-resolution x-ray diffraction mapping

technique. However, the technique is not sensitive to single misfit dislocations but rather to the average relaxation of the strain. This leads easily to the overestimation of the critical thickness. In this thesis, two kinds of x-ray methods were used for sample characterization.

High-resolution x-ray diffraction (HRXRD) was used to determine the thickness and the composition of the grown epitaxial layers and synchrotron x-ray topography was used to detect misfit dislocations in the layers. These x-ray methods are based on the diffraction of x-rays from the lattice planes of the crystalline sample [87]. The angle of diffraction is dependent on the x-ray wavelength and the distance between the lattice planes. HRXRD uses an exact narrow-band x-ray source, which enables an accurate resolving of the lattice constant of the sample by measuring the diffraction angle. A modular Philips X'Pert Pro diffractometer was used for the HRXRD studies in this thesis. The synchrotron x-ray topography [88, 89] uses a wide spectrum of x-ray wavelengths, which leads to a number of diffracted topographs of the sample in different diffraction angles. The topography technique is very sensitive to the strain and thus the strain field generated by a single misfit dislocation can be detected. The topographs were recorded with a high-resolution photographic film in a back-reflection geometry as illustrated in figure 13. The synchrotron x-ray beam was directed to the sample perpendicular to the sample surface through a hole in the photographic film. Then, photographs were taken from the small topographs (1 mm × 0.75 mm) using an optical microscope and a camera. The topography measurements were performed at the Hamburger Synchrotronstrahlungslabor (HASYLAB) at the Deutches Elektronen-Synchrotron (DESY) in Hamburg, Germany, utilizing the continuous spectrum

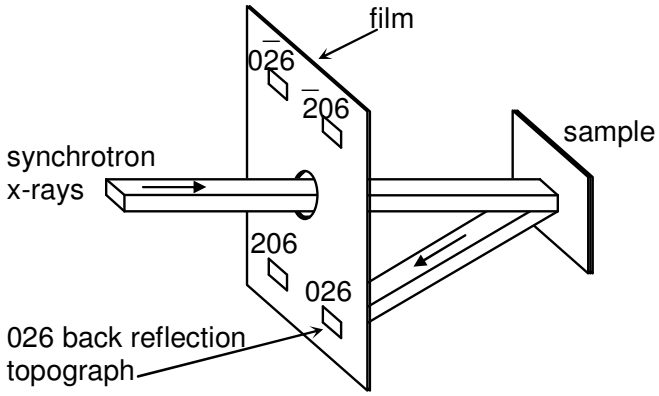

Figure 13. Back-reflection geometry in synchrotron x-ray topography. Several topographs of different lattice planes are recorded to film with single exposure due to wide spectrum of x-ray wavelengths.

of synchrotron radiation from a DORIS III storage-ring bending-magnet and from an x-ray undulator.

The strain relaxation mechanism in the strained $GaAs_{1-x}N_x$ on GaAs structures was studied in publication VI. In epilayers thicker than the critical thickness, an isotropic and a uniform misfit cross-hatched dislocation network along two mutually perpendicular <1 1 0> directions was observed. As the total strain was further increased when increasing the N composition or the epilayer thickness, the dislocations accumulated and the strain relaxation was found to continue through the cracks in the epilayer. However, some areas of the epilayer still remain highly strained. Figure 14 shows AFM images and synchrotron x-ray topographs of $GaAs_{0.965}N_{0.035}$ epilayers having a thickness of 80 nm and 220 nm on GaAs substrate. Single dislocations can be detected with both techniques as shown in figures 14(a) and 14(b). In topography, a much larger area is studied at once, which makes it more sensitive in dislocation detection than AFM. Figures 14(c) and 14(d) show the AFM image and the topograph for the 220 nm thick epilayer. The accumulation of dislocations is shown in the AFM image. The topograph shows, in addition to the dislocations, some broad white lines. They were confirmed to be cracks by AFM and optical microscopy.

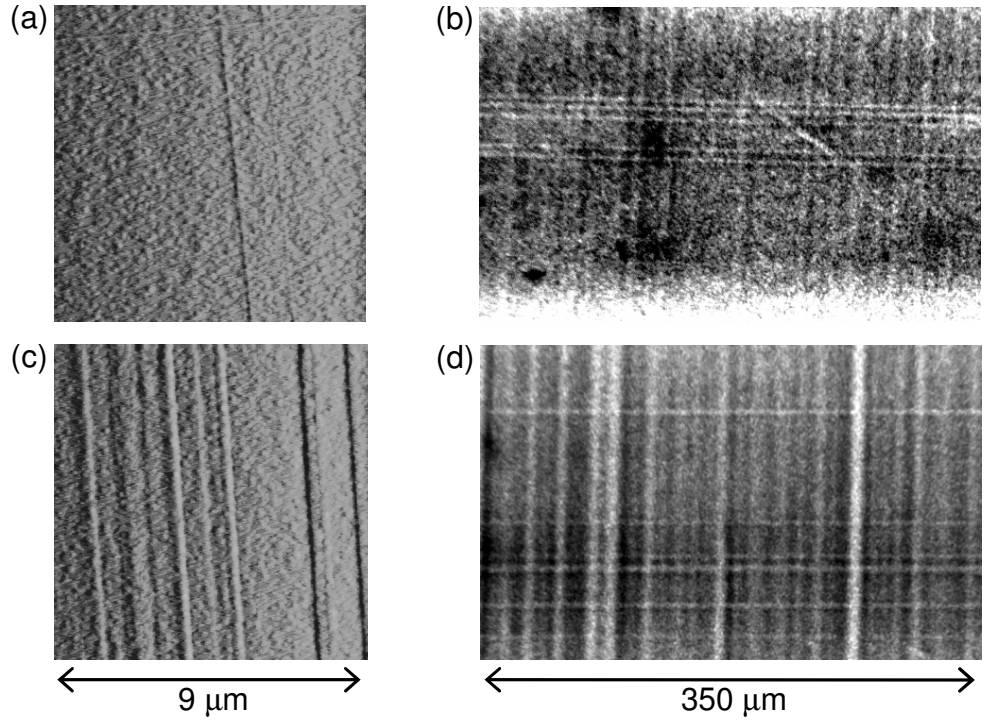

Figure 14. (a) Atomic force micrograph and (b) topograph of an 80-nm-thick $GaAs_{0.965}N_{0.035}$ epilayer on GaAs. Similar pictures (c-d) for a 220-nm-thick $GaAs_{0.965}N_{0.035}$ epilayer on GaAs. Scale in height is approximately 1 nm from dark to bright color for AFM images.

The critical thickness for $GaAs_{1-x}N_x$ on GaAs was determined with the two N compositions of x = 0.009 and x = 0.035. For the 500-nm-thick $GaAs_{1-x}N_x$ epilayer with x = 0.009 a very low misfit dislocation density was found, which indicates that the epilayer thickness slightly exceeded the critical thickness. For the $GaAs_{0.965}N_{0.035}$ epilayer the critical thickness was found to be between 50 nm and 80 nm. The values obtained for the critical thickness are about two times larger than the theoretical prediction [86]. Also Uesugi, Morooka, and Suemune found that the critical thickness for $GaAs_{1-x}N_x$ on GaAs is larger than predicted by the theory [86]. They were able to grow coherent epilayers having a thickness of up to six times the theoretical critical thickness. However, the values obtained in this thesis show that the real critical thickness is smaller than the one obtained by the HRXRD determination of the relaxation state.

4.3 Point defects

Intrinsic point defects are atomic perturbations in the lattice. $GaAs_{1-x}N_x$ is organized to the wurtzite lattice, where the gallium atoms should be bound to four neighboring group-V atoms (figure 15(a)). Typical intrinsic point defects are antisites, vacancies and interstitials, and they always exist in the materials. Their density is dependent on the formation probabilities during the growth. The growth conditions are optimized to keep the intrinsic defect concentration low. Impurities are another type of point defects. The concentrations of the impurities are dependent on the growth conditions, the type of precursors and the purity of source materials. Typical impurities are carbon, oxygen and hydrogen.

The point defects may have electronic states in the band gap and thus have severe effects on the electronic properties of the semiconductors. The effects of the defects are pronounced when the mean distance between the defects is shorter than the diffusion length of the carriers. Typically the defect concentrations below 10^{14} cm^{-3} are not a concern. The point defects can be harmful in several ways. Some defects trap carriers, some act as nonradiative recombination centers, and some just disturb the carrier transport by increasing the carrier scattering.

Several kinds of point defects have been reported to exist in arsenide-nitrides. The degradation of the photoluminescence intensity [90] and the carrier transport properties [91, 92] with increasing N composition indicate the increasing concentration of nonradiative recombination centers and carrier traps. The formation of the defects is specific to the growth conditions and thus the consistent identification of these defects has been difficult. However, the following point defects are identified in arsenide-nitrides: As_{Ga} antisites, N

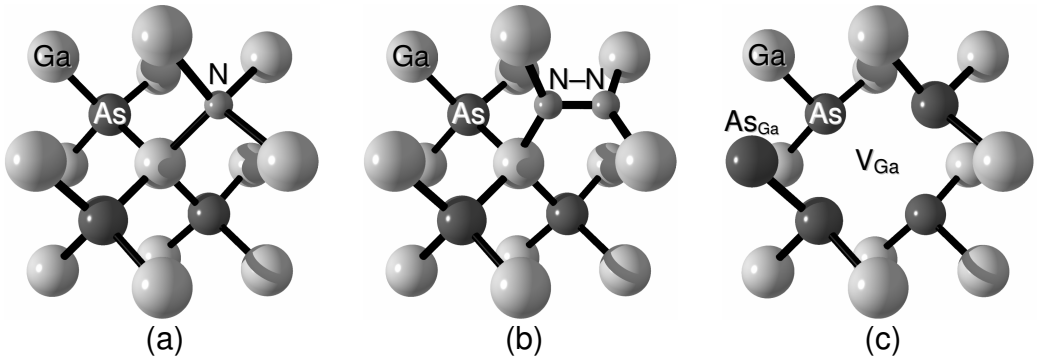

Figure 15. Illustration of (a) substitutional N, (b) N–N split interstitial, and (c) Ga vacancy and As antisite.

interstitials, Ga vacancies, and impurities like oxygen, carbon, and hydrogen. As_{Ga} antisites (figure 15(c)) were found from MBE-grown material in the optically detected magnetic resonance studies and their density was found to decrease during annealing [93, 94]. N interstitials were found in the MBE-grown material by an ion-channeling technique and their concentration also decreased during annealing [12, 95, 96]. Zhang and Wei [19] showed with thermodynamic calculations that the N–N split interstitial (figure 15(b)) has relatively low formation energy and that it forms a midgap electron state. Ga vacancies (figure 15(c)) were found in the MBE-grown material [96], and also in the MOVPE-grown material in this thesis. The Ga vacancies in the MOVPE-grown arsenide-nitrides are discussed in detail in the following section. The high concentrations of impurities are reported mainly for the MOVPE-grown materials. Oxygen was found to form a midgap nonradiative recombination center [97]. Carbon is known to act as a p-type dopant, and the incorporation of carbon is enhanced in arsenide-nitrides [63, 76]. Hydrogen is found in MOVPE-grown materials in large quantities and the high concentration of hydrogen was also found to remain after annealing [76]. Thus, hydrogen is strongly bonded to the lattice. However, the role of hydrogen to the material properties is not clear. Hydrogen was found to passivate nitrogen in the MBE-grown arsenide-nitrides hydrogenated after the growth [98, 99]. The effect was lost after annealing, which means that hydrogen is in a different configuration in the MOVPE-grown arsenide-nitrides.

4.4 Gallium vacancies

In publication VII, the vacancies in the MOVPE-grown $GaAs_{1-x}N_x$ were studied with positron annihilation spectroscopy in Doppler-broadening mode [100]. Figure 16(a) shows the principle of the measurement technique. A monoenergetic positron beam was directed to the sample and the beam energy was varied to scan the depth profile. Positrons thermalize very fast in the sample and diffuse until they annihilate with electrons or are trapped. At room

temperature, the positrons are effectively trapped by neutral and negatively charged vacancy defects due to the missing positive atom core. In annihilation, two gamma photons are created with energies of about 511 keV. The annihilation spectrum of trapped positrons differs from that of free positrons by a smaller Doppler-broadening. Figure 16(b) shows the determination of the line shape parameters S and W as a fraction of counts in the central area and the wing area of the peak, respectively. Due to the smaller Doppler broadening, vacancies are detected as an increase in the low-momentum parameter S and a decrease in the high-momentum parameter W. The different vacancy defects have different annihilation line shapes and thus characteristic S and W parameters are observed for the defects. The measurement is sensitive in the vacancy density range approximately from 10^{16} cm^{-3} to 10^{19} cm^{-3}.

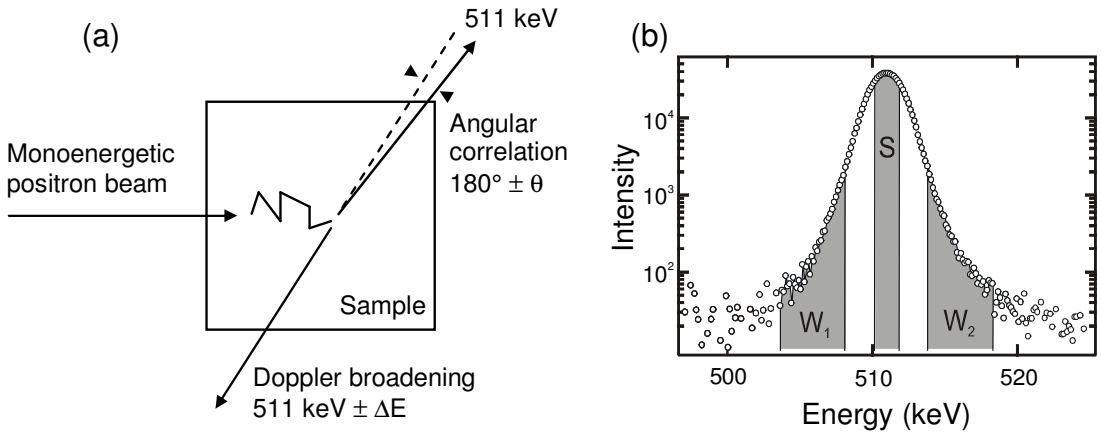

Figure 16. (a) Annihilation of positron with electron of solid sample. (b) Example of positron annihilation spectrum and illustration of determination of S and W parameters.

An increase of the S parameter and a decrease of the W parameter were observed for $GaAs_{1-x}N_x$ with increasing N composition. The behavior of the positron annihilation line shape is a clear indication of vacancy defects. Figure 17 shows the measured W and S parameters for four $GaAs_{1-x}N_x$ samples with different N composition x. The data is in line between a vacancy-free p-type GaAs reference and reference samples containing high density of Ga vacancies. Figure 17 shows also the characteristic values for As vacancies. Even though the determination of the characteristic values for the vacancies is difficult and has some uncertainties, the data shows the vacancies to be Ga vacancies. The MOVPE-grown arsenide-nitrides were found to be p-type, which supports the assumption of the vacancies being Ga vacancies. Arsenic vacancies are not typically seen with positron annihilation spectroscopy in p-type GaAs, because of their positive charge. However, Corbel et al. [103] showed that Ga vacancies

are not stable in the GaAs lattice at temperatures above 300°C and the $GaAs_{1-x}N_x$ samples were grown at > 500°C. Thus, the detected Ga vacancies have to form defect complexes with some other defects or impurities. We suggest that a possible defect complex is formed from a Ga vacancy and a group-V antisite due their opposite charge. The concentration of the Ga vacancies was found to anticorrelate with photoluminescence intensity before and after annealing. The anticorrelation suggests that the defect complex containing Ga vacancy acts as a nonradiative recombination center.

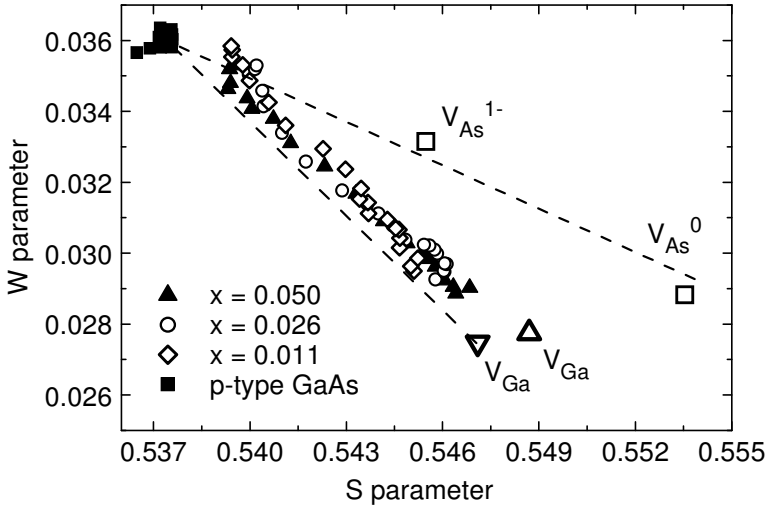

Figure 17. High-momentum parameter W as a function of low-momentum parameter S for as grown $GaAs_{1-x}N_x$ samples [Publ. VII]. Characteristic W and S parameters for V_{As} (□) and V_{Ga} (Δ) are from Refs. 101 and 102, respectively, and parameters for V_{Ga} (∇) are measured in this work. Dashed lines are guides to eye.

5 OPTICAL PROPERTIES

The optical properties of arsenide-nitrides at different temperatures were studied using photoluminescence. Section 5.1 describes the luminescence properties of $GaAs_{1-x}N_x$ and the effect of the post-growth treatments on the luminescence properties are discussed in section 5.2. Section 5.3 introduces the photoreflectance measurements of $GaAs_{1-x}N_x$ bulk and quantum well layers and discusses the energy difference between the two structures.

5.1 Luminescence

The luminescence properties of materials are typically studied with photoluminescence (PL) methods, where free carriers are excited to the material with high-energy photons. The carriers thermalize rapidly (in picoseconds) to the energy states in the band edges and then luminescence from electronic transitions over the energy band can be detected. The luminescence is dispersed with an optical grating and the spectrum of the luminescence is detected with a proper light detector.

$GaAs_{1-x}N_x$ shows luminescence properties that are typical for materials exhibiting exciton localization at the band edges due to potential fluctuations [104]. The spectral shape of the luminescence changes at different temperatures. The photoluminescence (PL) peak has an exponential low-energy tail at low temperatures < 200 K [29], which is caused by the energy distribution of the density of the localized states below the conduction band edge. At higher temperatures > 300 K the PL peak has a typical high-energy tail caused by the emission from the thermally populated delocalized states of the energy band. The transition from the localized exciton emission to the band edge emission with increasing temperature causes an S-shaped behavior for the PL peak energy as a function of the temperature [105]. The PL emission is strongly dependent on the excitation power. Not only the PL intensity, but also the PL peak energy shifts at low temperatures, because of the state filling of the localized states. The PL peak energy increases when the PL intensity increases, and vise versa. Long PL decay times have been measured for arsenide-nitrides at low temperatures [23, 105]. The PL decay times of over 4 ns have been found for the localized states in the low-energy tail, whereas the high-energy edge of the PL peak exhibits a decay time of less than 500 ps. The short decay time at the high-energy edge of the PL peak is attributed to the diffusion of the delocalized excitons to the rapid nonradiative centers. At room temperature such a behavior

is not found. The whole PL peak exhibits about the same decay time of several hundreds of picoseconds [105]. At high N compositions the decay time shortens due to the increasing concentration of the nonradiative defects.

Figure 18 shows an example of PL spectra at temperatures of 15 K and 300 K. The sample is a 5-nm-thick $GaAs_{0.967}N_{0.033}$ quantum well (QW) on GaAs with the GaAs cap having a thickness of 50 nm. The MOVPE-growth was done at 530°C with the growth rate of 1.1 μm/h and the TBAs/III ratio of 4. The composition was determined using x-ray diffraction of a 500-nm-thick layer grown with the same parameters. The PL was excited using the 488 nm line of an argon ion laser with the relatively large intensity of 200 W/cm^2. At room temperature the PL peak has a high-energy tail caused by the thermal population of the carriers.

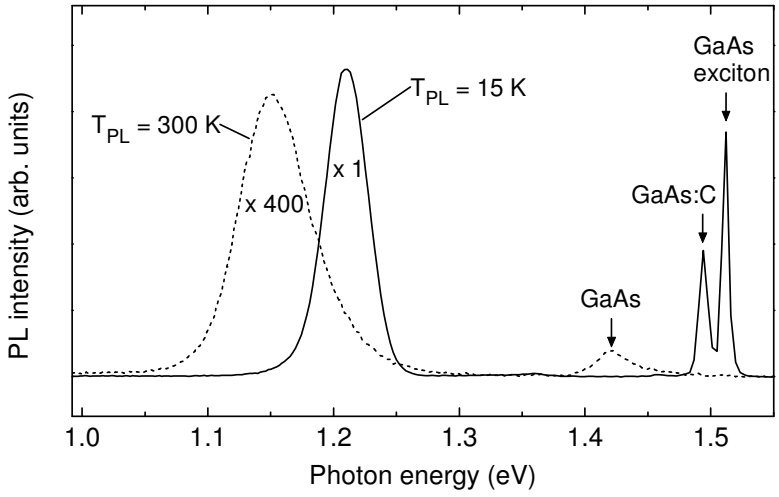

Figure 18. Photoluminescence spectra of annealed $GaAs_{0.967}N_{0.033}$/GaAs quantum well sample at temperatures of 15 K and 300 K. Quantum well thickness is 5 nm.

At the temperature of 15 K the intensity of the PL is about 400 times higher than at room temperature and the shift between the peaks is about 60 meV. The low-energy tail of the PL peak at low temperatures was used to estimate the localization potential E_o [24]. The exponential energy distribution of the density-of-states denoted as $\rho(E) \propto e^{E/E_o}$ was fitted to the low-energy tail. The localization potential of 16 meV was found to describe the $GaAs_{1-x}N_x$/GaAs QWs in publication VIII. The small localization potential indicates a good composition homogeneity of $GaAs_{1-x}N_x$. Indeed, McKay et al. [106] studied the N distribution in $GaAs_{1-x}N_x$ grown in similar conditions as in this thesis and

found that N was randomly distributed. Only the number of the nearest-neighbor N pairs was slightly enhanced compared to the random distribution.

5.2 Post-growth treatments

Despite the reasonably good structural properties of $GaAs_{1-x}N_x$, the PL intensity degrades rapidly with increasing N composition. This has been attributed to the increasing concentration of nonradiative point defects in the material. Thus, Rao et al. [107] used a large excitation intensity in the PL studies of arsenide-nitrides and found that the PL intensity is greatly enhanced after laser treatment or thermal annealing. With growth optimization and thermal annealing the optical quality of GaInNAs has developed to be comparable to that of conventional InGaAs [108]. The both post-growth treatments, laser treatment and thermal annealing, have been studied in this thesis.

In publication VIII, the effect of laser treatment on the PL intensity of $GaAs_{1-x}N_x$ was studied. The excitation intensities over 50 W/cm^2 caused permanent changes in the material. Figure 19 shows the effect of the laser treatment with increasing treatment intensity. The PL excitation intensity was the same 42 W/cm^2 for all the spectra. The irradiation was done at 15 K temperature for 60 seconds prior to the measurement of the PL spectrum. The PL intensity increases rapidly with increasing laser treatment intensity and then saturates at laser treatment intensities over 10^4 W/cm^2. The shift in the PL peak

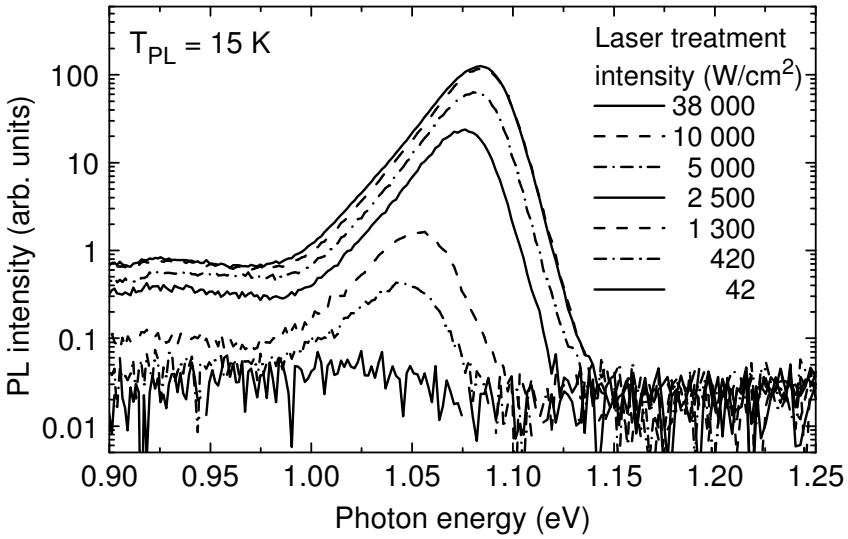

Figure 19. Photoluminescence spectra measured at 15 K before and after laser treatments of $GaAs_{0.955}N_{0.045}$/GaAs quantum well having thickness of 5 nm [Publ. VIII]. PL excitation intensity was 42 W/cm^2 for all spectra.

energy with increasing PL intensity is due to the state filling of localized states, which again is the consequence of decreased concentration of nonradiative recombination centers. Overall, the effect of laser treatment should be noticed when operating with large excitation intensities.

In publications I and IV, the thermal annealing was studied for the $GaAs_{1-x}N_x$ and $Ga_{1-y}In_yN_xAs_{1-x}$ quantum wells, respectively. Annealing was performed in the MOVPE reactor. The optimum annealing conditions for the maximum PL intensity were at 700°C for 10 minutes using a TBAs excess in H_2 carrier gas. The annealed samples exhibited an increased luminescence intensity and a shift in the PL peak energy toward higher energies as compared to the as-grown samples. The increased PL intensity is due to the decreased concentration of nonradiative centers. The shift in the PL peak energy is pronounced in GaInNAs, where a local rearrangement of the N neighboring atoms is found to occur during the annealing [109]. In GaAsN the small shift in the PL peak energy is due to the state filling of the localized states similarly as in case of laser treatment.

Figure 20 shows the PL spectra of a 5-nm-thick $GaAs_{0.967}N_{0.033}$/GaAs QW with different post-growth treatments. The luminescence of the QW was at the spectral range of 1.1–1.25 eV. The annealed sample exhibited an enhanced PL intensity as compared to the as-grown sample over the whole measured spectral range, whereas the PL intensity of the laser treated sample was enhanced only at the spectral range of below 1.25 eV. This is due to the different nature of the treatments. In annealing, the whole lattice gains thermal energy, which allows

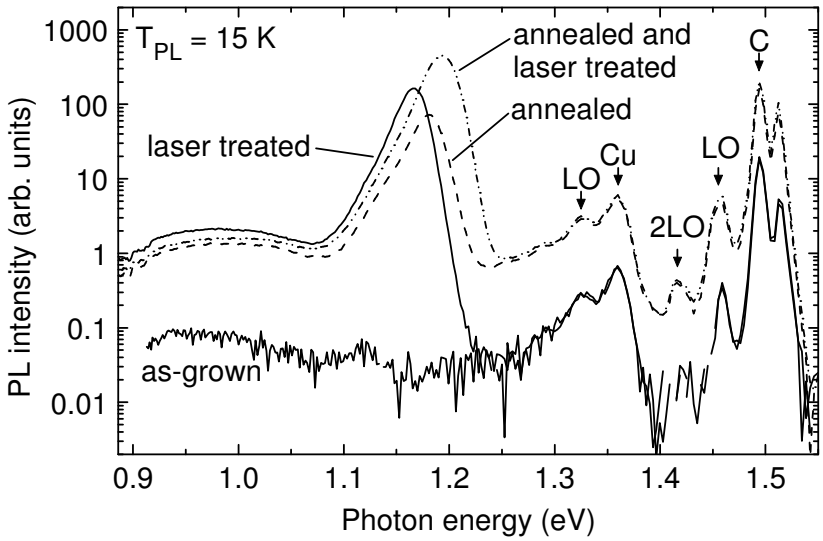

Figure 20. Photoluminescence spectra of 5-nm-thick $GaAs_{0.967}N_{0.033}$/GaAs quantum well before and after different post-growth treatments.

the rearrangement of atomic configuration in the material. The laser treatment affects the defects in the lattice most likely because of recombination enhanced defect reactions [107, 110]. A high density of carriers is generated in the material and the carriers focus their energy on the volumes with the fastest recombination channels. Thus, the changes in the atomic configurations are possible only in the vicinity of the fast nonradiative recombination centers, where the band gap energy E_g is transformed into the lattice vibration energy by a series of coherent carrier captures. The laser treatment is a precision tool for specific defects. The largest PL intensity was obtained by using the both post-growth treatments.

The spectra in figure 20 show many typical details about the optical properties of MOVPE-grown $GaAs_{1-x}N_x$. The PL intensity of the as-grown sample was very small and an enhancement of the orders of magnitudes was observed in the PL intensity after a post-growth treatment. A broad luminescence peak below the QW peak in energy was observed. It is related to the defect states in $GaAs_{1-x}N_x$ and its PL intensity was enhanced in the post-growth treatments. However, the intensity was only about the hundredth part of the QW luminescence intensity. The spectral features above 1.25 eV in energy were attributed to GaAs related, because their intensity did not change in the laser treatment. The laser treatment affects the carrier density in the GaAsN QW only. The peak at 1.512 eV was caused by excitons in GaAs and the peak at 1.494 eV was related to the carbon impurity state in GaAs. The concentration of carbon is increased in GaAs grown at low temperatures and thus the intensity of the peak was relatively high and two LO-phonon replicas were observed. The origin of the peak at 1.36 eV is presumably the copper impurities in GaAs [111] having similar optical properties with carbon impurity. In publication I the peak at 1.36 eV was attributed to the diffused N in the GaAs barriers. That is an unlikely explanation for the peak, because no other PL peaks of the dilute N concentration in the GaAs barriers have been found. The small shift in energy between the annealed and laser treated QW peaks was likely due to the growth nonuniformity in the sample.

A remarkable difference between the two post-growth treatments for GaInNAs was found in publication VIII. Annealing shifts the PL peak energy of GaInNAs for 86 meV toward higher energies due to the local rearrangement of atoms, whereas the shift after the laser treatment was negligible. Thus, laser treatment could offer advantages over annealing in the long-wavelength GaInNAs structures, where the blue shift of the PL peak should be avoided.

5.3 Photoreflectance

The energy band structure of the $GaAs_{1-x}N_x$ layers was studied with photoreflectance. In the photoreflectance method the electric field of the material is modulated with an absorbing laser beam and the reflectance spectrum is measured simultaneously [112]. The modulation of the electric field changes the energies of the electron states in the material, which causes changes to the reflectance spectrum at energies of the absorbing transitions. Thus, the energies of the optical transitions are detected.

Figure 21 shows the lowest transition energies observed from 500-nm-thick $GaAs_{1-x}N_x$ bulk layers and 5-nm-thick $GaAs_{1-x}N_x$ quantum wells with the N composition x of from 0% to 4.5%. The difference in the transition energy between the bulk layer and the quantum well is due to the quantization energy of the carriers in the quantum well. Figure 21 shows that the quantization energy increases as the N composition x increases. This is partly due to the increasing confinement potential ($E_{g,GaAs} - E_{g,GaAsN}$). The fitting of the data with the conventional potential well model leads inevitably to a decreasing electron effective mass with increasing N composition x from 0.9% to 4.5%. The similar results were reported by Zhang et al. [31]. However, Skierbiszewski et al. [39] showed that the strong non-parabolic nature of the conduction band prevents the use of the conventional potential well model, which assumes parabolic bands. They explained the data of Zhang et al. by means of the band anticrossing model (see section 2.3), which predicts the gradually increasing electron effective mass with increasing N composition x.

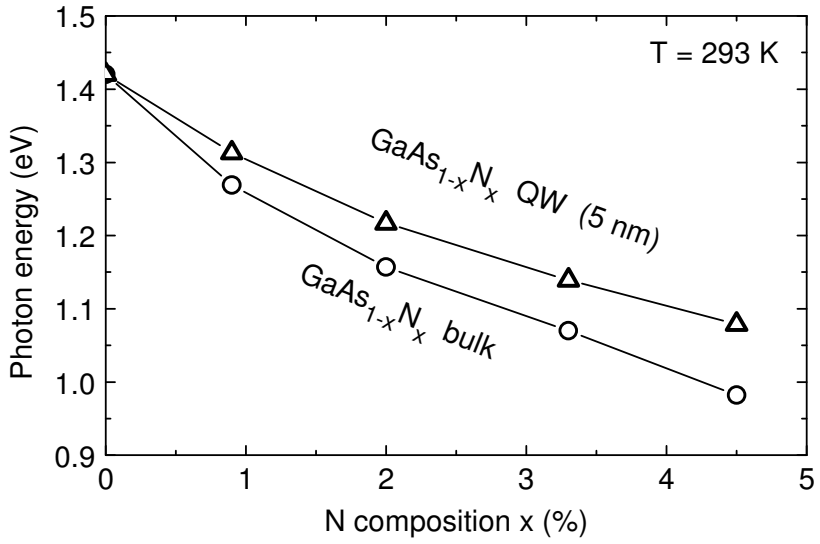

Figure 21. Transition energies of 500-nm-thick $GaAs_{1-x}N_x$ bulk layer and 5-nm-thick $GaAs_{1-x}N_x$ quantum well (QW) on GaAs as a function of N composition x.

6 GaInNAs

Quantum dots and the novel $Ga_{1-y}In_yN_xAs_{1-x}$ material are used in the low-bang-gap device applications on GaAs. The high N compositions are not used in the components due to the negative impact of N to the properties of the material. Section 6.1 describes the applications of lattice matched $Ga_{1-y}In_yN_xAs_{1-x}$ and discusses the growth and the electrical properties of the alloy. Section 6.2 introduces $Ga_{1-y}In_yN_xAs_{1-x}$ quantum wells and their use in semiconductor lasers. The combination of the quantum dots and the $Ga_{1-y}In_yN_xAs_{1-x}$ material is discussed in the section 6.3.

6.1 Bulk layers

The quaternary alloy $Ga_{1-y}In_yN_xAs_{1-x}$ is a significant addition to the selection of the III–V compound semiconductors. There exist no other compound with a low band gap that can be lattice matched to GaAs. $Ga_{1-y}In_yN_xAs_{1-x}$ is lattice matched to GaAs when $y \approx 3x$. The novel quaternary alloy allows the tuning of the band gap for thick layers on GaAs from 1.42 eV to below 1 eV. Device applications like multijunction solar cells and heterojunction bipolar transistors benefit from such a possibility. The novel compound allows the enhancement of the total efficiency of the multijunction solar cells [113] and the reduction of the turn-on voltage of the heterojunction bipolar transistors [114]. The electrical and optical properties of $Ga_{1-y}In_yN_xAs_{1-x}$ are similar to those of $GaAs_{1-x}N_x$ including the defect problems with increasing N composition x. The fast nonradiative recombination in $Ga_{1-y}In_yN_xAs_{1-x}$ reduces the minority-carrier diffusion length and is also a major concern for electrical applications like solar cells and transistors [113].

Adding of indium to $GaAs_{1-x}N_x$ further complicates the MOVPE growth procedure. A rapid decrease in the N incorporation efficiency was found with increasing In content of the $Ga_{1-y}In_yN_xAs_{1-x}$ alloy [115]. However, with the MBE growth technique the In and N compositions can be controlled independently [74, 116]. The reason for the dependency between the In and N compositions in MOVPE is not clear, but the effects like surface reconstruction [117] and stronger Ga–N bond over In–N bond combined with the indium segregation on the surface [115] have been reported. Recently, NF_3 was found to be an effective N source that strongly reduces the dependency between the In and N compositions [64].

The effects of post-growth annealing are also more complicated on $Ga_{1-y}In_yN_xAs_{1-x}$ than on $GaAs_{1-x}N_x$. Kurtz et al. [118] reported that mainly Ga–N bonds were found from as-grown $Ga_{1-y}In_yN_xAs_{1-x}$ and after annealing a signal form In–N bond raised, which implies atomic changes in the N neighbors during annealing. Klar et al. [109] showed with samples having a large In composition of $y = 0.3$ that after annealing at high temperatures the N occurs at In rich environments. They proposed that the Ga–N bonds are favored at the surface during the growth and that appropriate annealing leads to In rich configurations of N due to the dominance of local strain effects in the bulk.

The doping of the lattice matched $Ga_{1-y}In_yN_xAs_{1-x}$ grown by MBE was studied in publication II. The unintentional doped material was n-type, having a free electron concentration of $5 \times 10^{15}\,cm^{-3}$. The n-type and p-type alloys were doped with Si and Be, respectively. The carrier concentrations were observed to decrease substantially with increasing N content in both n- and p-type materials. After annealing the carrier concentration of the p-type material recovered, whereas that of the n-type material remained low. The mobility of the carriers was also decreased with increasing N content. Annealing slightly recovered the carrier mobility in both n- and p-type materials.

Figure 22(a) shows the hole concentration of MOVPE-grown $Ga_{1-y}In_yN_xAs_{1-x}$ as a function of the N composition x. The layers were lattice matched to GaAs and unintentionally p-type doped with carbon. The carbon incorporation from precursors is enhanced at low growth temperatures. The hole

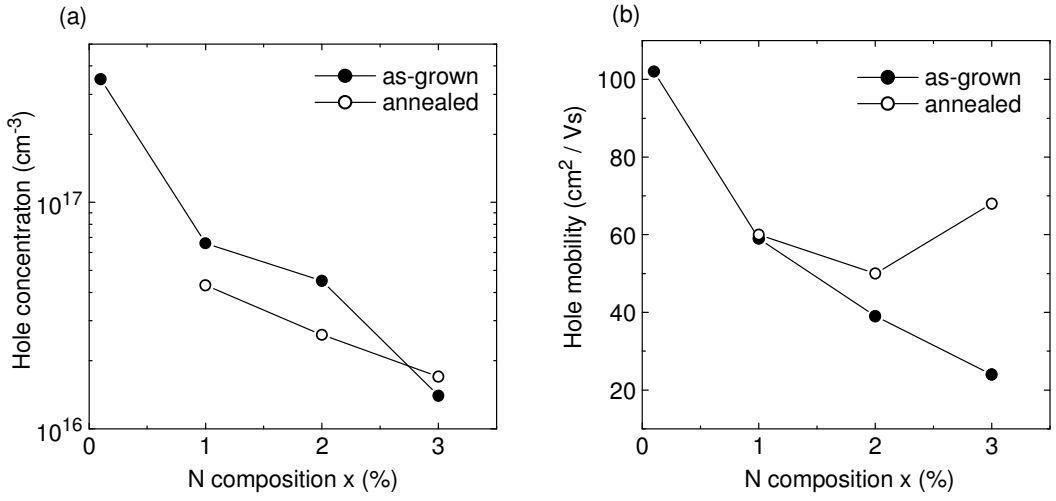

Figure 22. Hole (a) concentration and (b) mobility as a function of N composition x in $Ga_{1-y}In_yN_xAs_{1-x}$ epilayers lattice-matched ($y \approx 3x$) to GaAs.

concentration was found to decrease with increasing N content and to be unchanged during annealing. This is presumably due to the carrier compensation by a donor type defect that is not affected by annealing. The most likely candidate for the defect is H donor impurity [119]. The high concentration of the H impurity was reported to remain during annealing [76]. Also the mobility of the holes in $Ga_{1-y}In_yN_xAs_{1-x}$ was found to degrade with increasing N composition x. A slight recovery of the mobility was found after annealing. This is probably due to the decreased defect concentration by annealing.

6.2 Quantum wells

The potential of $Ga_{1-y}In_yN_xAs_{1-x}$ as an active material in the long-wavelength quantum well (QW) lasers on GaAs has been the driving force of the research of arsenide-nitrides. Typically, the $Ga_{1-y}In_yN_xAs_{1-x}$ quantum wells are highly compressively strained due to the large In composition y from 0.2 to 0.4. The transition energy of a $Ga_{1-y}In_yN_xAs_{1-x}$ QW with x = 0 can be tuned from 1.42 eV to below 1.1 eV. However, the strain prevents the high quality QWs with transition energies below 1 eV, and thus N has to be introduced to achieve the telecommunication wavelengths of 1.3 μm and 1.55 μm at the photon energies of 0.95 eV and 0.80 eV, respectively.

In publication IV, the MOVPE growth conditions for the $Ga_{1-y}In_yN_xAs_{1-x}$ quantum wells were studied. The incorporation of N from dimethylhydrazine was very difficult when the In composition y was 0.3 and larger. Thus, the lowest transition energies were obtained with In compositions around 0.23. Figure 23 shows the room-temperature photoluminescence spectra of the $Ga_{1-y}In_yN_xAs_{1-x}$ quantum wells annealed at 700°C for 10 minutes. The luminescence intensity decreases rapidly with increasing N composition x. Thus, a nitrogen composition as low as possible should be used for the device applications. The 1.3 μm and 1.55 μm emission wavelengths require the N compositions of 1–2% and 3–4%, respectively.

Laser structures were grown using three $Ga_{1-y}In_yN_xAs_{1-x}$ quantum wells with y = 0.2 and x < 0.02 buried in GaAs in the active layer. The active layer was grown between 1.5-μm-thick $Al_{0.32}Ga_{0.68}As$ waveguide layers on n-type doped substrate. When excited with femtosecond laser pulses, the lasers with x = 0.01–0.02 exhibit threshold excitation intensities of about 7 times larger than the reference laser structure with x = 0. The $Ga_{1-y}In_yN_xAs_{1-x}$ quantum wells showed very different optical properties inside the laser structures from the test samples grown on undoped semi-insulating GaAs without the laser structure. Two reasons were suggested. First, $Ga_{1-y}In_yN_xAs_{1-x}$ is very sensitive to the growth temperature and the doped substrates have a slightly different surface temperature than the undoped substrates. Second, the AlGaAs layer under the

active layer was found to decrease the N composition. This might be due to the difference in the surface reconstruction of Al(Ga)As and GaAs [117, 120].

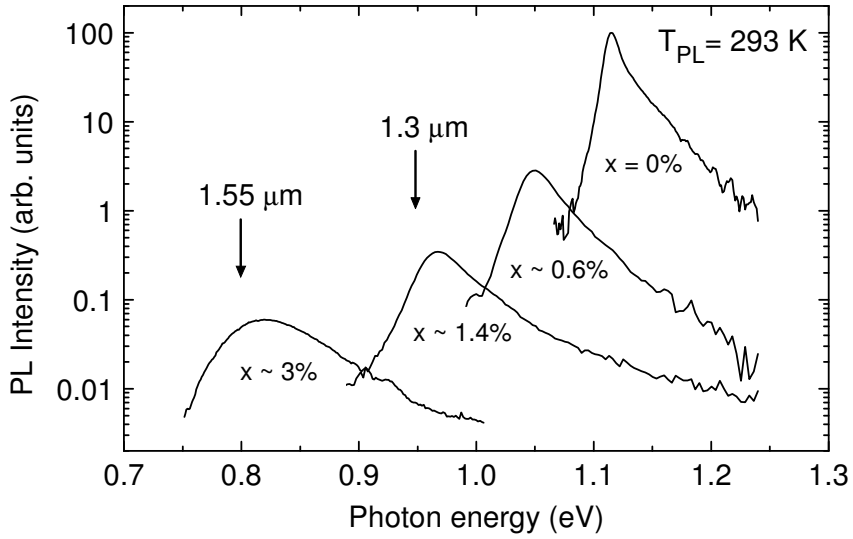

Figure 23. Room-temperature photoluminescence spectra of 6-nm-thick $Ga_{0.68}In_{0.32}N_xAs_{1-x}$ quantum wells with x = 0, x = 0.006, and x = 0.014. Also spectrum of 9-nm-thick $Ga_{0.74}In_{0.26}N_{0.03}As_{0.97}$ quantum well is shown.

6.3 Quantum dots

In(Ga)As quantum dots are extensively studied for the GaAs-based telecommunication lasers as an active material operating at 1.3 μm wavelength [1, 121]. The quantum dots are self-assembled three-dimensional In(Ga)As islands formed on GaAs due to strain effects when the epilayer thickness exceeds the critical thickness. However, the islands are coherently strained on GaAs and thus exhibit excellent optical properties. Figure 24 shows the typical size of the islands. The homogeneity and the size distribution of the islands can be controlled with the growth parameters like the growth temperature, the growth rate and the V/III-ratio. The challenge in the quantum dot growth for lasers is to obtain a homogenous distribution of proper sized islands with a high areal density. The densities from 10^{10} cm^{-2} to 10^{11} cm^{-2} are required for the lasers to realize a sufficient optical gain at quantum dot ground state energy.

The quantum dot structures and the $Ga_{1-y}In_yN_xAs_{1-x}$ material are both used to reach long-wavelength operation on GaAs. Sopanen et al. [122] combined the two materials using MBE and achieved a room-temperature photoluminescence at 1.52 μm wavelength. In publication III, the growth of the $Ga_{1-y}In_yN_xAs_{1-x}$

quantum dots by MOVPE was studied. The N incorporation from dimethylhydrazine to the islands was found to be negligible due to the high In composition $y > 0.45$ needed for the island formation. However, the use of dimethylhydrazine during the growth was found to be useful, because it turned to act as an independent tuning parameter for the island formation. The areal density of the islands was increased by up to one order of magnitude as compared to that of the respective GaInAs islands and the size of the islands was controlled with the dimethylhydrazine flow. An enhanced room-temperature photoluminescence was observed at 1.3 μm wavelength from the quantum dot samples grown with dimethylhydrazine.

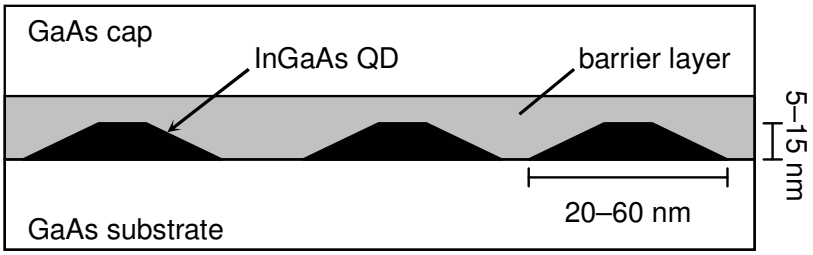

Figure 24. Schematic illustration of InGaAs quantum dots on GaAs. Quantum dots are buried in barrier layer.

The covering of the $In_{0.5}Ga_{0.5}As$ quantum dots with a $Ga_{1-y}In_yN_xAs_{1-x}$ barrier layer was studied in publication V. The barrier layer on the islands is illustrated in figure 24. The barrier layer decreases the carrier confinement energy and reduces the strain in the quantum dots [123]. Thus, the energy states of the quantum dots are decreased. The N incorporation into the $In_{0.15}Ga_{0.85}As$ barrier layer with MOVPE is much easier than into the $In_{0.5}Ga_{0.5}As$ islands due to the lower In composition in the barrier layer. The wavelength and the intensity of the photoluminescence increased at the vicinity of 1.3 μm wavelength when $Ga_{0.85}In_{0.15}N_xAs_{1-x}$ was used as a barrier layer instead of $In_{0.15}Ga_{0.85}As$. The N composition x was not determined, but according to previous studies it was about 0.02. When the N composition in the barrier layer was further increased, a type II band alignment was observed. The conduction band edge of the $Ga_{0.85}In_{0.15}N_xAs_{1-x}$ barrier layer decreased below that of the $In_{0.5}Ga_{0.5}As$ quantum dots.

7 SUMMARY

The long-wavelength emission on GaAs substrates has motivated the study of quantum dots and the novel $Ga_{1-y}In_yN_xAs_{1-x}$ material. Both of the methods are developing rapidly and the commercial products utilizing them are about to emerge on the market. However, a lot of work is still needed to bring these technologies to their full potential. In this thesis, the N incorporation from dimethylhydrazine (DMHy) into $Ga_{1-y}In_yN_xAs_{1-x}$ by MOVPE was studied and the $Ga_{1-y}In_yN_xAs_{1-x}$ material was combined with the quantum dot technology. The electrical, structural, and optical properties of $Ga_{1-y}In_yN_xAs_{1-x}$ were studied with various experimental techniques.

The incorporation efficiency of N into GaAs is very low and thus the MOVPE growth of $GaAs_{1-x}N_x$ requires carefully optimized growth conditions. The record high N composition x of 0.056 for the $GaAs_{1-x}N_x$ quantum wells was achieved using a low growth temperature of 530°C and a low TBAs/III-ratio of 2. The similar growth conditions combined with an extremely high DMHy/V-ratio of 0.97 and the In composition y of 0.26 for the $Ga_{1-y}In_yN_xAs_{1-x}$ quantum wells were used to obtain the 1.61 μm wavelength emission on GaAs substrate.

The luminescence intensity of $Ga_{1-y}In_yN_xAs_{1-x}$ decreased rapidly with increasing N composition and thus the post-growth treatments were studied to recover the luminescence intensity. A reasonable luminescence intensity at the wavelength of 1.38 μm from a $GaAs_{0.944}N_{0.056}$ quantum well structure was obtained at a low temperature of 9 K using post-growth annealing in the MOVPE reactor at 700°C for 10 minutes. The similar annealing treatment resulted in a room-temperature luminescence at 1.51 μm wavelength from a $Ga_{0.74}In_{0.26}N_{0.03}As_{0.97}$ quantum well structure. The enhancement of the luminescence intensity due to annealing was typically orders of magnitudes. The laser treatment was found to be as effective as annealing in increasing the photoluminescence intensity of the $GaAs_{1-x}N_x$ quantum wells. However, a difference between the two post-growth methods was found for the $Ga_{1-y}In_yN_xAs_{1-x}$ quantum wells. A negligible blue shift was observed after the laser treatment as compared to that after annealing. The novel phenomenon is advantageous when reaching long wavelengths with $Ga_{1-y}In_yN_xAs_{1-x}$.

The electrical properties of lattice matched $Ga_{1-y}In_yN_xAs_{1-x}$ with $y \approx 3x$ grown by MBE and MOVPE were studied. The MBE-grown n- and p-type alloys were doped with Si and Be, respectively. The carrier concentrations were

observed to decrease substantially with increasing N content in both n- and p-type materials. After annealing the carrier concentration of the p-type material recovered, whereas that of the n-type material remained low. The MOVPE-grown $Ga_{1-y}In_yN_xAs_{1-x}$ was found to be unintentionally p-doped presumably due to carbon impurities. The free carrier concentration decreased with increasing N composition x and was not affected by annealing.

A good structural quality of the $GaAs_{1-x}N_x$ layers was observed as long as the layer thickness was smaller than the critical thickness. The critical thickness was determined with two N compositions of x = 0.009 and x = 0.035. For the 500-nm-thick $GaAs_{1-x}N_x$ epilayer with x = 0.009 the thickness slightly exceeded the critical thickness. For the $GaAs_{0.965}N_{0.035}$ epilayer, the critical thickness was between 50 nm and 80 nm. The values obtained for the critical thickness are about twice as large as the theoretical prediction. The vacancy-type point defects in MOVPE-grown $GaAs_{1-x}N_x$ were studied for the first time and an increasing concentration of Ga vacancies was found with increasing N composition x. The anticorrelation between the photoluminescence intensity and the vacancy concentration was attributed to nonradiative recombination through the defect complexes containing the Ga vacancies.

The growth of the $Ga_{1-y}In_yN_xAs_{1-x}$ quantum dots by MOVPE and the use of $Ga_{1-y}In_yN_xAs_{1-x}$ as a barrier layer for the InGaAs quantum dots were studied. The use of dimethylhydrazine during the quantum dot growth increased the areal density of the islands by up to one order of magnitude as compared to that of the respective GaInAs islands, and the dimethylhydrazine flow was found to control the size of the islands. An enhanced room-temperature photoluminescence was observed at 1.3 µm wavelength from the quantum dot samples grown with dimethylhydrazine. Also the benefit of $Ga_{1-y}In_yN_xAs_{1-x}$ as a barrier layer for the InGaAs quantum dots was shown.

REFERENCES

[1] O. B. Shchekin and D. G. Deppe, *1.3 μm InAs quantum dot laser with T_o = 161 K from 0 to 80°C*, Appl. Phys. Lett. **80**, 3277 (2002).

[2] M. Weyers, M. Sato and H. Ando, *Red shift of photoluminescence and absorption in dilute GaAsN alloy layers*, Jpn. J. Appl. Phys. **31**, L853 (1992).

[3] M. Kondow, K. Uomi, A. Niwa, T. Kitatani, S. Watahiki and Y. Yazawa, *GaInNAs: A novel material for long-wavelength-range laser diodes with excellent high-temperature performance*, Jpn. J. Appl. Phys. **35**, 1273 (1996).

[4] A. Ramakrishnan, G. Steinle, D. Supper, C. Degen and G. Ebbinghaus, *Electrically pumped 10 Gbit/s MOVPE-grown monolithic 1.3 μm VCSEL with GaInNAs active region*, Electron. Lett. **38**, 322 (2002).

[5] D. J. Wolford, J. A. Bradley, K. Fry, and J. Thompson, in *Proceedings of the 17th International Conference on the Physics of Semiconductors*, edited by J. D. Chadi and W. A. Harrison (Springer, New York, 1984), p. 627.

[6] X. Liu, M.-E. Pistol, L. Samuelson, S. Schwetlick, and W. Seifert, *Nitrogen pair luminescence in GaAs*, Appl. Phys. Lett. **56**, 1451 (1990).

[7] X. Liu, M.-E. Pistol, and L. Samuelson, *Excitons bound to nitrogen pairs in GaAs*, Phys. Rev. B **42**, 7504 (1990).

[8] M. Weyers and M. Sato, *Growth of GaAsN alloys by low-pressure metalorganic chemical vapor deposition using plasma-cracked NH_3*, Appl. Phys. Lett. **62**, 1396 (1993).

[9] S. A. Ding, S. R. Barman, K. Horn, H. Yang, B. Yang, O. Brandt, and K. Ploog, *Valence band discontinuity at a cubic GaN/GaAs heterojunction measured by synchrotron-radiation photoemission spectroscopy*, Appl. Phys. Lett. **70**, 2407 (1997).

[10] L. Bellaiche, S.-H. Wei, and A. Zunger, *Localization and percolation in semiconductor alloys: GaAsN vs GaAsP*, Phys. Rev. B **54**, 17 568 (1996).

[11] Y. Zhang, A. Mascarenhas, H. P. Xin, and C. W. Tu, *Valence-band splitting and shear deformation potential of dilute $GaAs_{1-x}N_x$ alloys*, Phys. Rev. B **61**, 4433 (2000).

[12] S. G. Spruytte, C. W. Coldren, J. S. Harris, W. Wampler, P. Krispin, K. Ploog, and M. C. Larson, *Incorporation of nitrogen in nitride-arsenides: Origin of improved luminescence efficiency after anneal*, J. Appl. Phys. **89**, 4401 (2001).

[13] W. J. Fan, S. F. Yoon, T. K. Ng, S. Z. Wang, W. K. Loke, R. Liu, and A. Wee, *Comparison of nitrogen compositions in the as-grown GaN_xAs_{1-x} on GaAs measured by high-resolution x-ray diffraction and secondary-ion mass spectroscopy*, Appl. Phys. Lett. **80**, 4136 (2002).

[14] G. B. Stringfellow, *Calculation of solubility and solid-gas distribution coefficient of N in GaP*, J. Electrochem. Soc. **119**, 1780 (1972); G. B. Stringfellow and G. Horn, J. Electrochem. Soc. **124**, 1806 (1977).

[15] I. Ho and G. B. Stringfellow, *Solubility of nitrogen in binary III-V systems*, J. Cryst. Growth **178**, 1 (1997).

[16] Y. Qiu, S. A. Nikishin, H. Temkin, V. A. Elyukhin and Yu. A. Kudriavtsev, *Thermodynamic considerations in epitaxial growth of $GaAs_{1-x}N_x$ solid solutions*, Appl. Phys. Lett. **70**, 2831 (1997).

[17] W. G. Bi and C. W. Tu, *Bowing parameter of the band-gap energy of GaN_xAs_{1-x}*, Appl. Phys. Lett. **70**, 1608 (1997).

[18] D. Schlenker, T. Miyamoto, Z. Pan, F. Koyama, and K. Iga, *Miscibility gap calculation for $Ga_{1-x}In_xN_yAs_{1-y}$ including strain effects*, J. Cryst. Growth **196**, 67 (1999).

[19] S. B. Zhang and Su-Huai Wei, *Nitrogen solubility and induced defect complexes in epitaxial GaAs:N*, Phys. Rev. Lett. **86**, 1789 (2001).

[20] S. Francoeur, S. A. Nikishin, C. Jin, Y. Qiu, and H. Temkin, *Excitons bound to nitrogen clusters in GaAsN*, Appl. Phys. Lett. **75**, 1538 (1999).

[21] P. R. C. Kent, L. Bellaiche, and A. Zunger, *Pseudopotential theory of dilute III–V nitrides*, Semicond. Sci. Technol. **17**, 851 (2002).

[22] H. Grüning, L. Chen, Th. Hartmann, P. J. Klar, W. Heimbrodt, F. Höhnsdorf, J. Koch, and W. Stolz, *Optical spectroscopic studies of N-related bands in Ga(N,As)*, phys. stat. sol. (b) **215**, 39 (1999).

[23] I. A. Buyanova, W. M. Chen, G. Pozina, J. P. Bergman, B. Monemar, H. P. Xin, and C. W. Tu, *Mechanism for low-temperature photoluminescence*

in GaNAs/GaAs structures grown by molecular-beam epitaxy, Appl. Phys. Lett. **75**, 501 (1999).

[24] Y.G.Hong and C.W.Tu, *Optical properties of GaAs/GaN_xAs_{1-x} quantum well structures grown by migration-enhanced epitaxy*, J. Cryst. Growth **242**, 29 (2002).

[25] I. A. Buyanova, G. Pozina, P. N. Hai, N. Q. Thinh, J. P. Bergman, W. M. Chen, H. P. Xin, and C. W. Tu, *Mechanism for rapid thermal annealing improvements in undoped GaN_xAs_{1-x}/GaAs structures grown by molecular beam epitaxy*, Appl. Phys. Lett. **77**, 2325 (2000).

[26] I. A. Buyanova, W. M. Chen, G. Pozina, B. Monemar, H. P. Xin, and C. W. Tu, *Mechanism for light emission in GaNAs/GaAs structures grown by molecular beam epitaxy*, phys. stat. sol. (b) **216**, 125 (1999).

[27] U. Tisch, E. Finkman, and J. Salzman, *The anomalous bandgap bowing in GaAsN*, Appl. Phys. Lett. **81**, 463 (2002).

[28] I. Suemune, K. Uesugi, W. Walukiewicz, *Role of nitrogen in the reduced temperature dependence of band-gap energy in GaNAs*, Appl. Phys. Lett. **77**, 3021 (2000).

[29] A. Polimeni, M. Bissiri, A. Augieri, G. Baldassarri Höger von Högersthal, M. Capizzi, D. Gollub, M. Fischer, M. Reinhardt, and A. Forchel, *Reduced temperature dependence of the band gap in $GaAs_{1-y}N_y$ investigated with photoluminescence*, Phys. Rev. B **65**, 235325 (2002).

[30] C. Skierbiszewski, P. Perlin, P. Wisniewski, W. Knap, T. Suski, W. Walukiewicz, W. Shan, K. M. Yu, J. W. Ager, E. E. Haller, J. F. Geisz, and J. M. Olson, *Large, nitrogen-induced increase of the electron effective mass in $In_yGa_{1-y}N_xAs_{1-x}$*, Appl. Phys. Lett. **76**, 2409 (2000).

[31] Y. Zhang, A. Mascarenhas, H. P. Xin, and C. W. Tu, *Formation of an impurity band and its quantum confinement in heavily doped GaAs:N*, Phys. Rev. B **61**, 7479 (2000).

[32] P. N. Hai, W. M. Chen, I. A. Buyanova, H. P. Xin, and C. W. Tu, *Direct determination of electron effective mass in GaNAs/GaAs quantum wells*, Appl. Phys. Lett. **77**, 1843 (2000).

[33] C. Skierbiszewski, P. Perlin, P. Wisniewski, T. Suski, J. F. Geisz, K. Hingerl, W. Jantsch, D. E. Mars, and W. Walukiewicz, *Band structure and optical properties of $In_yGa_{1-y}As_{1-x}N_x$ alloys*, Phys. Rev. B **65**, 035207 (2001).

[34] W. Shan, W. Walukiewicz, J. W. Ager III, E. E. Haller, J. F. Geisz, D. J. Friedman, J. M. Olson, and Sarah R. Kurtz, *Band Anticrossing in GaInNAs Alloys*, Phys. Rev. Lett. **82**, 1221 (1999).

[35] J. D. Perkins, A. Mascarenhas, Yong Zhang, J. F. Geisz, D. J. Friedman, J. M. Olson, and Sarah R. Kurtz, *Nitrogen-activated transitions, level repulsion, and band gap reduction in* $GaAs_{1-x}N_x$ *with* $x < 0.03$, Phys. Rev. Lett. **82**, 3312 (1999).

[36] K. M. Yu, W. Walukiewicz, W. Shan, J. W. Ager III, J. Wu, E. E. Haller, J. F. Geisz, D. J. Friedman, and J. M. Olson, *Nitrogen-induced increase of the maximum electron concentration in group III-N-V alloys*, Phys. Rev. B **61**, R13337 (2000).

[37] J. Wu, W. Shan, W. Walukiewicz, K. M. Yu, J. W. Ager III, E. E. Haller, H. P. Xin, and C. W. Tu, *Effect of band anticrossing on the optical transitions in* $GaAs_{1-x}N_x$*/GaAs multiple quantum wells*, Phys. Rev. B **64**, 085320 (2001).

[38] M. Hofmann, A. Wagner, C. Ellmers, C. Schlichenmeier, S. Schäfer, F. Höhnsdorf, J. Koch, W. Stolz, S. W. Koch, W. W. Rühle, J. Hader, J. V. Moloney, E. P. O'Reilly, B. Borchert, A. Yu. Egorov, and H. Riechert, *Gain spectra of (GaIn)(NAs) laser diodes for the 1.3-*μ*m-wavelength regime*, Appl. Phys. Lett. **78**, 3009 (2001).

[39] C. Skierbiszewski, S. P. Lepkowski, P. Perlin, T. Suski, W. Jantsch, J. Geisz, Effective mass and conduction band dispersion of GaAsN/GaAs quantum wells, Physica E **13**, 1078 (2002).

[40] W. Shan, W. Walukiewicz, K. M. Yu, J. W. Ager III, E. E. Haller, J. F. Geisz, D. J. Friedman, J. M. Olson, Sarah R. Kurtz, H. P. Xin, and C. W. Tu, *Band anticrossing in III–N–V alloys*, phys. stat. sol. (b) **223**, 75 (2001).

[41] C. Skierbiszewski, *Experimental studies of the conduction-band structure of GaInNAs alloys*, Semicond. Sci. Technol. **17**, 803 (2002).

[42] E. P. O'Reilly and A. Lindsay, $k \cdot P$ *Model of Ordered* GaN_xAs_{1-x}, phys. stat. sol. (b) **216**, 131 (1999).

[43] E. P. O'Reilly, A. Lindsay, S. Tomic, and M. Kamal-Saadi, *Tight-binding and* $k \cdot p$ *models for the electronic structure of Ga(In)NAs and related alloys*, Semicond. Sci. Technol. **17**, 870 (2002).

[44] P. J. Klar, H. Grüning, W. Heimbrodt, J. Koch, W. Stolz, P. M. A. Vicente, A. M. Kamal Saadi, A. Lindsay, and E. P. O'Reilly, *Pressure and*

temperature dependent studies of GaN_xAs_{1-x}/GaAs quantum well structures, phys. stat. sol. (b) **223**, 163 (2001).

[45] J. Hader, S. W. Koch, J. V. Moloney, and E. P. O'Reilly, *Influence of the valence-band offset on gain and absorption in GaNAs/GaAs quantum well lasers*, Appl. Phys. Lett. **76**, 3685 (2000).

[46] J. Hader, S. W. Koch, J. V. Moloney, and E. P. O'Reilly, *Gain in 1.3 μm materials: InGaNAs and InGaPAs semiconductor quantum-well lasers*, Appl. Phys. Lett. **77**, 630 (2000).

[47] J. R. Chelikowsky and M. L. Cohen, *Electronic structure of silicon*, Phys. Rev. B **10**, 5095 (1974).

[48] R. M. Martin, *Elastic properties of ZnS structure semiconductors*, Phys. Rev. B **1**, 4005 (1970).

[49] L. Bellaiche, Su-Huai Wei, and Alex Zunger, *Composition dependence of interband transition intensities in GaPN, GaAsN, and GaPAs alloys*, Phys. Rev. B **56**, 10233 (1997).

[50] P. R. C. Kent and Alex Zunger, *Theory of electronic structure evolution in GaAsN and GaPN alloys*, Phys. Rev. B **64**, 115208 (2001).

[51] T. Mattila, Su-Huai Wei, and Alex Zunger, *Localization and anticrossing of electron levels in $GaAs_{1-x}N_x$ alloys*, Phys. Rev. B **60**, R11245 (1999).

[52] I. Gorczyca, C. Skierbiszewski, T. Suski, N. E. Christensen, and A. Svane, *Pressure and composition dependence of the electronic structure of $GaAs_{1-x}N_x$*, Phys. Rev. B **66**, R081106 (2002).

[53] H. Manasevit and W. Simpson, *The use of metalorganics in the preparation of semiconductor materials I. epitaxial gallium-V compounds*, J. Electrochem. Soc. **116**, 1725 (1969).

[54] J.-T. Zettler, K. Haberland, M. Zorn, M. Pristovsek, W. Richter, P. Kurpas and M. Weyers, *Real-time monitoring of MOVPE device growth by reflectance anisotropy spectroscopy and related optical techniques*, J. Cryst. Growth **195**, 151 (1998).

[55] M. Heimbuch, A. Holmes, C. Reaves, M. Mack, S. Denbaars and L. Coldren, *Tertiarybutylarsine and tertiarybutylphosphine for the MOCVD growth of low-threshold 1.55-μm $In_xGa_{1-x}As$/InP quantum-well lasers*, J. Electron. Mater. **23**, 87 (1994).

[56] W. Stolz, *Alternative N-, P- and As-precursors for III/V-epitaxy*, J. Cryst. Growth **209**, 272 (2000).

[57] R. M. Lum and J. K. Klingert, *Thermochemistry of alkylarsine compounds used as arsenic precursors in metalorganic vapor phase epitaxy*, J. Appl. Phys. **66**, 3820 (1989).

[58] R. T. Lee and G. B. Stringfellow, Pyrolysis of 1,1 dimethylhydrazine for OMVPE growth, J. Electron. Mater. **28**, 963 (1999).

[59] Y. Qiu, C. Jin, S. Francoeur, S. A. Nikishin, and H. Temkin, *Metalorganic molecular beam epitaxy of GaAsN with dimethylhydrazine*, Appl. Phys. Lett. **72**, 1999 (1998).

[60] C. Jin, S. A. Nikishin, V. I. Kuchinskii, H. Temkin, and M. Holtz, *Metalorganic molecular beam epitaxy of (In)GaAsN with dimethylhydrazine*, J. Appl. Phys. **91**, 56 (2002).

[61] E. Bourret-Courchesne, Q.Ye, D. W. Peters, J. Arnold, M. Ahmed, S. J. C. Irvine, R. Kanjolia, L. M. Smith, S. A. Rushworth, *Pyrolysis of dimethylhydrazine and its co-pyrolysis with triethylgallium*, J. Cryst. Growth **217**, 47 (2000).

[62] Sarah Kurtz, R. Reedy, Greg D. Barber, J. F. Geisz, D. J. Friedman, W. E. McMahon, and J. M. Olson, *Incorporation of nitrogen into GaAsN grown by MOCVD using different precursors*, J. Cryst. Growth **234**, 318 (2002).

[63] Sarah Kurtz, R. Reedy, B. Keyes, Greg D. Barber, J. F. Geisz, D. J. Friedman, W. E. McMahon, and J. M. Olson, *Evaluation of NF3 versus dimethylhydrazine as N sources for GaAsN*, J. Cryst. Growth **234**, 323 (2002).

[64] A. J. Ptak, Sarah Kurtz, C. Curtis, R. Reedy, and J. M. Olson, *Incorporation effects in MOCVD-grown (In)GaAsN using different nitrogen precursors*, J. Cryst. Growth **243**, 231 (2002).

[65] X. Wei, G. H. Wang, G. Z. Zhang, X. P. Zhu, X. Y. Ma, and L. H. Chen, *Metalorganic chemical vapor deposition of GaNAs alloys using different Ga precursors*, J. Cryst. Growth **236**, 516 (2002).

[66] Koji Takahashi, Yoshitaka Tomomura, Hiroaki Ikeda, and Hidenori Kawanishi, *Molecular-beam epitaxy of (Al)GaAsN using ammonia as the nitrogen source*, Appl. Phys. Lett. **78**, 1364 (2001).

[67] M. Kondow, K. Uomi, K. Hosomi, and T. Mozume, *Gas-source molecular beam epitaxy of GaN_xAs_{1-x} using a N radical as the N source*, Jpn. J. Appl. Phys. **33**, L1056 (1994).

[68] S. G. Spruytte, M. C. Larson, W. Wampler, C. W. Coldren, H. E. Petersen, J. S. Harris, *Nitrogen incorporation in group III–nitride–*

arsenide materials grown by elemental source molecular beam epitaxy, J. Cryst. Growth **227-228**, 506 (2001).

[69] A. Ougazzaden, Y. Le Bellego, E. V. K. Rao, M. Juhel, L. Leprince, and G. Patriarche, *Metal organic vapor phase epitaxy growth of GaAsN on GaAs using dimethylhydrazine and tertiarybutylarsine*, Appl. Phys. Lett. **70**, 2861 (1997).

[70] S. Sato, Y. Osawa, T. Saitoh, and I. Fujimura, *Room-temperature pulsed operation of 1.3 μm GaInNAs/GaAs laser diode*, Electron. Lett. **33**, 1386 (1997).

[71] Katsuhiro Uesugi and Ikuo Suemune, *Metalorganic molecular beam epitaxy of GaNAs alloys on (0 0 1)GaAs*, J. Cryst. Growth **189/190**, 490 (1998).

[72] U. W. Pohl, C. Möller, K. Knorr, W. Richter, J. Gottfriedsen, H. Schumann, K. Rademann, and A. Fielicke, *Tertiarybutylhydrazine: a new precursor for the MOVPE of group III-nitrides*, Mat. Sci. Eng. B **59**, 20 (1999).

[73] G.-Y. Plaine, C. Asplund, P. Sundgren, S. Mogg, and M. Hammar, *Low-temperature metal-organic vapor-phase epitaxy growth and performance of 1.3-μm GaInNAs/GaAs single quantum well lasers*, Jpn. J. Appl. Phys. **41**, 1040 (2002).

[74] V. A. Odnoblyudov, A. Yu. Egorov, A. R. Kovsh, A. E. Zhukov, N. A. Maleev, E. S. Semenova, and V. M. Ustinov, *Thermodynamic analysis of the MBE growth of GaInAsN*, Semicond. Sci. Technol. **16**, 831 (2001).

[75] B. K. Tanner, P. J. Parbrook, C. R. Whitehouse, A. M. Keir, A. D. Johnson, J. Jones, D. Wallis, L. M. Smith, B. Lunn, and J. H. C. Hogg, *In situ x-ray topography measurement of the growth temperature dependence of the critical thickness of epitaxial InGaAs on GaAs*, J. Phys. D: Appl. Phys. **34**, A109 (2001).

[76] A. Moto, M. Takahashi, S. Takagishi, *Hydrogen and carbon incorporation in GaInNAs*, J. Cryst. Growth **221**, 485 (2000).

[77] F. Höhnsdorf, J. Koch, C. Agert, W. Stolz, *Investigations of (GaIn)(NAs) bulk layers and (GaIn)(NAs)/GaAs multiple quantum well structures grown using tertiarybutylarsine (TBAs) and 1,1-dimethylhydrazine (UDMHy)*, J. Cryst. Growth **195**, 391 (1998).

[78] M. Kawaguchi, T. Miyamoto, E. Gouardes, D. Schlenker, T. Kondo, F. Koyama, and K. Iga, *Optical quality dependende on growthh rate for*

metalorganic chemical vapor deposition grown GaInNAs/GaAs, Jpn. J. Appl. Phys. **39**, L1219 (2000).

[79] F. Alexandre, E. Gouardes, O. Gauthier-Lafaye, N. Bouadma, A. Vuong, and B. Thedrez, *Nitride-based long-wavelength lasers on GaAs substrates*, J. Mater. Sci.: Mater. El. **13**, 633 (2002).

[80] G. Zimmermann, A. Ougazzaden, A. Gloukhian, E. V. K. Rao, D. Delprat, A. Ramdane, and A. Mircea, *The role of N_2 and H_2 as carrier gas on the selective area MOVPE of InP-based heterostructures using TBAs and TBP as group-V sources*, Mat. Sci. Eng. B **44**, 37 (1997).

[81] A. Ougazzaden, E. Rao, B. Sermage, L. Leprince, and M. Gauneau, *High-quality InGaAsN growth by metalorganic vapor-phase epitaxy using nitrogen carrier gas and dimethylhydrazine, tertiarybutylarsine as group V precursors*, Jpn. J. Appl. Phys. **38**, 1019 (1999).

[82] Steven R. Kurtz, N. A. Modine, E. D. Jones, A. A. Allerman, and J. F. Klem, *Insights into the electronic properties of InGaAsN: the effect of nitrogen from band structure to devices*, Semicond. Sci. Technol. **17**, 843 (2002).

[83] I. Suemune, K. Uesugi, and T.-Y. Seong, *Growth and structural characterization of III–N–V semiconductor alloys*, Semicond. Sci. Technol. **17**, 755(2002).

[84] B. V. Volovik, A. R. Kovsh, W. Passenberg, H. Kuenzel, N. Grote, N. A. Cherkashin, Yu G. Musikhin, N. N. Ledentsov, D. Bimberg, and V. M. Ustinov, *Optical and structural properties of self-organized InGaAsN/GaAs nanostructures*, Semicond. Sci. Technol. **16**, 186 (2001).

[85] K. Uesugi, N. Morooka, and I. Suemune, *Reexamination of N composition dependence of coherently grown GaNAs band gap energy with high-resolution x-ray diffraction mapping measurements*, Appl. Phys. Lett. **74**, 1254 (1999).

[86] K. Uesugi, N. Morooka, and I. Suemune, *Strain effect on the N composition dependence of GaNAs bandgap energy grown on (0 0 1) GaAs by metalorganic molecular beam epitaxy*, J. Cryst. Growth **201/202**, 355 (1999).

[87] Paul F. Fewster, *X-ray scattering from semiconductors*, Imperial College Press, London, 2000.

[88] T. Tuomi, K. Naukkarinen, and P. Rabe, *Use of synchrotron radiation in x-ray diffraction topography*, Phys. Status Solidi a **25**, 93 (1974).

[89] T. Tuomi, *Synchrotron X-ray topography of electronic materials*, J. Synchrotron Rad. **9**, 174 (2002).

[90] I. A. Buyanova, W. M. Chen, B. Monemar, H. P. Xin, and C. W. Tu, *Effect of growth temperature on photoluminescence of GaNAs/GaAs quantum well structures*, Appl. Phys. Lett. **75**, 3781 (1999).

[91] Steven R. Kurtz, A. A. Allerman, C. H. Seager, R. M. Sieg, and E. D. Jones, *Minority carrier diffusion, defects, and localization in InGaAsN, with 2% nitrogen*, Appl. Phys. Lett. **77**, 400 (2000).

[92] A. Fleck, B. J. Robinson, and D. A. Thompson, *Characterization of defects in doped InGaAsN grown by molecular-beam epitaxy*, Appl. Phys. Lett. **78**, 1694 (2001).

[93] N. Q. Thinh, I. A. Buyanova, P. N. Hai, W. M. Chen, H. P. Xin, and C. W. Tu, *Signature of an intrinsic point defect in* GaN_xAs_{1-x}, Phys. Rev. B **63**, 033203 (2001).

[94] N. Q. Thinh, I. A. Buyanova, W. M. Chen, H. P. Xin, and C. W. Tu, *Formation of nonradiative defects in molecular beam epitaxial* GaN_xAs_{1-x} *studied by optically detected magnetic resonance*, Appl. Phys. Lett. **79**, 3089 (2001).

[95] T. Ahlgren, E. Vainonen-Ahlgren, J. Likonen, W. Li, and M. Pessa, *Concentration of interstitial and substitutional nitrogen in* GaN_xAs_{1-x}, Appl. Phys. Lett. **80**, 2314 (2002).

[96] W. Li, M. Pessa, T. Ahlgren, and J. Dekker, *Origin of improved luminescence efficiency after annealing of Ga(In)NAs materials grown by molecular-beam epitaxy*, Appl. Phys. Lett. **79**, 1094 (2001).

[97] A. Balcioglu, R. K. Ahrenkiel, and D. J. Friedman, *Evidence of an oxygen recombination center in* $p^+ - n$ *GaInNAs solar cells*, Appl. Phys. Lett. **76**, 2397 (2000).

[98] G. Baldassarri H. v. H., M. Bissiri, A. Polimeni, M. Capizzi, M. Fischer, M. Reinhardt, and A. Forchel, *Hydrogen-induced band gap tuning of (InGa)(AsN)/GaAs single quantum wells*, Appl. Phys. Lett. **78**, 3472 (2001).

[99] M. Bissiri, G. Baldassarri Höger von Högersthal, A. Polimeni, V. Gaspari, F. Ranalli, M. Capizzi, A. Amore Bonapasta, F. Jiang, M. Stavola, D. Gollub, M. Fischer, M. Reinhardt, and A. Forchel, *Hydrogen-induced passivation of nitrogen in* $GaAs_{1-y}N_y$, Phys. Rev. B **65**, 235210 (2002).

[100] K. Saarinen, P. Hautojärvi, and C. Corbel, Positron annihilation spectroscopy of defects in semiconductors, in *Identification of Defects in*

Semiconductors, edited by M. Stavola, Academic Press, New York, 1998, p. 209.

[101] R. Ambigapathy, A. A. Manuel, P. Hautojärvi, K. Saarinen, and C. Corbel, *Positron-annihilation studies of neutral and negatively charged As vacancies in GaAs*, Phys. Rev. B **50**, 2188 (1994); J. Gebauer, R. Krause-Rehberg, C. Domke, Ph. Ebert, K. Urban, and T. Staab, *Direct identification of As vacancies in GaAs using positron annihilation calibrated by scanning tunneling microscopy*, Phys. Rev. B **63**, 045203 (2001).

[102] T. Laine, K. Saarinen, P. Hautojärvi, C. Corbel, and M. Missous, *Defects in GaAs grown by molecular-beam epitaxy at low temperatures: stoichiometry, doping, and deactivation of n-type conductivity*, J. Appl. Phys. **86**, 1888 (1999).

[103] C. Corbel, F. Pierre, K. Saarinen, P. Hautojärvi, and P. Moser, *Gallium vacancies and gallium antisites as acceptors in electron-irradiated semi-insulating GaAs*, Phys. Rev. B **45**, 3386 (1992).

[104] I. A. Buyanova, W. M. Chen, G. Pozina, P. N. Hai, B. Monemar, H. P. Xin, and C. W. Tu, *Optical properties of GaNAs/GaAs structures*, Mat. Sci. Eng. B **82**, 143 (2001).

[105] A. Kaschner, T. Lüttgert, H. Born, A. Hoffmann, A. Yu. Egorov, and H. Riechert, *Recombination mechanisms in GaInNAs/GaAs multiple quantum wells*, Appl. Phys. Lett. **78**, 1391 (2001).

[106] H. A. McKay, R. M. Feenstra, T. Schmidtling, and U. W. Pohl, *Arrangement of nitrogen atoms in GaAsN alloys determined by scanning tunneling microscopy*, Appl. Phys. Lett. **78**, 82 (2001).

[107] E. V. K. Rao, A. Ougazzaden, Y. Le Bellego, and M. Juhel, *Optical properties of low band gap $GaAs_{(1-x)}N_x$ layers: Influence of post-growth treatments*, Appl. Phys. Lett. **72**, 1409 (1998).

[108] S. Shirakata, M. Kondow and T. Kitatani, *Temperature-dependent photoluminescence of high-quality GaInNAs single quantum wells*, Appl. Phys. Lett. **80**, 2087 (2002).

[109] P. J. Klar, H. Grüning, J. Koch, S. Schäfer, K. Volz, W. Stolz, W. Heimbrodt, A. M. Kamal Saadi, A. Lindsay, and E. P. O'Reilly, *(Ga, In)(N, As)-fine structure of the band gap due to nearest-neighbor configurations of the isovalent nitrogen*, Phys. Rev. B **64**, 121203(R) (2001).

[110] Yuzo Shinozuka, *Mechanisms of capture- and recombination-enhanced defect reactions in semiconductors*, Physica B **308–310**, 506 (2001).

[111] Z. G. Wang, H. P. Gislason, and B. Monemar, *Acceptor associates and bound excitons in GaAs:Cu*, J. Appl. Phys. **58**, 230 (1985).

[112] O. J. Glembochi and B. V. Shanabrook, Photoreflectance spectroscopy of microstructures, in *The spectroscopy of semiconductors*, Semiconductors and semimetals, Vol. 36, edited by A. K. Willardson, A. C. Beer, E. R. Weber, Academic Press, San Diego, 1992, p. 221.

[113] J. F. Geisz and D. J. Friedman, *III–N–V semiconductors for solar photovoltaic applications*, Semicond. Sci. Technol. **17**, 769 (2002).

[114] P. M. Asbeck, R. J. Welty, C. W. Tu, H. P. Xin, and R. E. Welser, *Heterojunction bipolar transistors implemented with GaInNAs materials*, Semicond. Sci. Technol. **17**, 898 (2002).

[115] D. J. Friedman, J. F. Geisz, S. R. Kurtz, J. M. Olson, and R. Reedy, *Nonlinear dependence of N incorporation on In content in GaInNAs*, J. Cryst. Growth **195**, 438 (1998).

[116] J. C. Harmand, G. Ungaro, L. Largeau, and G. Le Roux, *Comparison of nitrogen incorporation in molecular-beam epitaxy of GaAsN, GaInAsN, and GaAsSbN*, Appl. Phys. Lett. **77**, 2482 (2000).

[117] S.B. Zhang and A. Zunger, *Surface-reconstruction-enhanced solubility of N, P, As, and Sb in III-V semiconductors*, Appl. Phys. Lett. **71**, 677 (1997).

[118] Sarah Kurtz, J. Webb, L. Gedvilas, D. Friedman, J. Geisz, J. Olson, R. King, D. Joslin, and N. Karam, *Structural changes during annealing of GaInAsN*, Appl. Phys. Lett. **78**, 748 (2001).

[119] A. Janotti, S. B. Zhang, Su-Huai Wei, and C. G. Van de Walle, *Effects of hydrogen on the electronic properties of dilute GaAsN alloys*, Phys. Rev. Lett **89**, 086403 (2002).

[120] J. Shen, P. Jiang, and X. Xie, The difference between the surface reconstructions of AlAs(001) and GaAs(001), Surf. Rev. Lett. **6**, 1167 (1999).

[121] M. Grundmann, N. N. Ledentsov, F. Hopfer, F. Heinrichsdorff, F. Guffarth, D. Bimberg, V. M. Ustinov, A. E. Zhukov, A. R. Kovsh, M. V. Maximov, Yu. G. Musikhin, J. A. Lott, N. D. Zhakharov, and P. Werner, *Long-wavelength quantum-dot lasers*, J. Mater. Sci.: Mater. El. **13**, 643 (2002).

[122] M. Sopanen, H. P. Xin, C. W. Tu, *Self-assembled GaInNAs quantum dots for 1.3 and 1.55 μm emission on GaAs*, Appl. Phys. Lett. **76**, 994 (2000).

[123] J. Bloch, J. Shah, W. S. Hobson, J. Lopata, S. N. G. Chu, *Room-temperature 1.3 μm emission from InAs quantum dots grown by metal organic chemical vapor deposition*, Appl. Phys. Lett. **75**, 2199 (1999).